((*E*)-1-((4-Fluorophenyl)diazenyl)naphthalen-2-ol as an innovative and efficient corrosion inhibitor for carbon steel in 1 M HCl solution: Electrochemical analysis coupled with electronic/atomic-scale computational simulations

E.H. Akroujai,[1] S. Chetioui,[2,3] N. Benzbiria,[4] A. Barrahi,[5] A. Chraka,[6] A. Djedouani,[7,8] S. Chtita,[9] S. Lazar,[10] I. Warad,[11] A. Bellaouchou,[5] M. Assouag[1] and A. Zarrouk[5]*

[1]Team of Innovative Materials and Mechanical Manufacturing Processes, ENSAM, University Moulay Ismail, B.P. 15290, Al Mansour, Meknes, Morocco
[2]Unité de Recherche de Chimie de l'Environnement et Moléculaire Structurale, (CHEMS), Faculté des Sciences Exactes, Département de Chimie, Université des Frères Mentouri, Constantine 1, Constantine 25000, Algérie
[3]Faculté de Technologie, Université Mohamed Boudiaf M'sila, Algérie
[4]Laboratory of Interface Materials and Environment, Faculty of Sciences Ain Chock, Hassan II University, B.P. 5366 Maârif, Casablanca, Morocco
[5]Laboratory of Materials, Nanotechnology, and Environment, Faculty of Sciences, Mohammed V University in Rabat, Morocco, PO. Box. 1014, Rabat, Morocco
[6]Materials and Interfacial Systems Laboratory, ERESI Team, Department of Chemistry, Faculty of Sciences, Abdelmalek Essaâdi University, Morocco
[7]Laboratoire de Physicochimie Analytique et Cristallochimie des Matériaux Organométalliques et Biomoléculaires, Université Constantine 1, 25000, Algérie
[8]Ecole Normale Supérieure de Constantine, Université Constantine 3, 25000, Algérie
[9]Laboratory of Analytical and Molecular Chemistry, Faculty of Sciences Ben M'Sik, Hassan II University of Casablanca, Morocco
[10]Laboratoire de Biochimie, Environnement & Agroalimentaire, URAC 36, Faculté des Sciences et techniques de Mohammedia Université Hassan II-Casablanca, Mohammedia, Morocco
[11]Department of Chemistry, AN-Najah National University, P.O. Box 7, Nablus, Palestine
**E-mail: azarrouk@gmail.com*

Abstract

In the current paper, potentiodynamic polarization (PDP), electrochemical impedance spectroscopy (EIS) were employed to evaluate (*E*)-1-((4-fluorophenyl)diazenyl)naphthalen-2-ol (E4FN) ability to operate as carbon steel (CS) corrosion inhibitor in molar HCl acid. Data derived from PDP plots reveal that E4FN has a mixed-type nature. EIS outcomes show that increasing E4FN concentration lead to 20 times increment of polarization resistance (R_p) and alters the double layer capacitance (C_{dl}) from 116.2 to 54 $\mu F \cdot cm^{-2}$. The addition of 10^{-3} M of E4FN into the solution exhibit a maximal inhibition efficacy of 94.8%. The thermodynamic

activation descriptors were also assessed as a function of E4FN concentration. The adsorption of the inhibitory molecule on CS substrate obey to Langmuir isotherm. To confirm the adsorption phenomenon, scanning electron microscopy (SEM) coupled to energy dispersive X-ray spectroscopy (EDS) and UV-Visible methods were used. Overall, the findings reveal that E4FN compound enables to obtain an adequate prevented surface and mitigate the corrosion rate. Finally, the theoretical studies based on quantum chemical analysis (*i.e.* density functional theory (DFT)) and Monte Carlo simulation were also performed for understanding the adsorption mechanism of E4FN onto Fe-surface.

Keywords: *azo function, corrosion, HCl, inhibitor, electrochemical methods, SEM/EDS, UV-Visible, DFT, Monte Carlo simulations.*

Received: August 13, 2023. Published: August 25, 2023 doi: 10.17675/2305-6894-2023-12-3-18

1. Introduction

Carbon steel (CS) is a low-carbon metal mostly used in several industrial applications, owing to its low cost and virtuous mechanical properties. This type of steel is tough and strong, though it cannot be readily hardened [1, 2]. Highly aggressive acids are frequently employed in industries for cleaning, descaling, pickling and petroleum well acidizing [3, 4]. Among these, hydrochloric acid generates an extremely corrosive medium for CS [5–7]. Hence, many researchers have been focusing on the investigation of practical and proficient approaches to mitigate CS corrosion in such hostile media [8–10]. Corrosion inhibitors have attracted much attention and have been applied to diminish and hinder the corrosion of metallic components [11–15]. For instance, Self-Assembled monolayers (SAMs created from phosphonic acids [16], silanes [17, 18] or electrochemical reduction of aryldiazonium salts [19, 20]) and organic compounds [21–23] (comprising electron rich centers as polar functional groups, double/triple links, aromatic ring (s) and/or side chain) exhibit high anti-corrosive properties. The occurrence of certain sets of atoms (O, N, S and P) or bonds (N=N, C=N, C=S, C=C, R–OH, *etc.*) in the molecular structure of an organic compound enables the inhibitor to adhere strongly to the metallic substrate [24–26]. In many instances, the inhibitory performance of these organic products is dictated by factors in the medium in which they operate, including the chemical properties of the metal, the inhibitor molecular structure and size, mode of adsorption and the electrochemical potential at the interface metal/medium [27]. Hence, several elements are taken into consideration before choosing any inhibitor namely its economical allowance, inhibiting potency and eco-friendly character [28]. Over the past few years, many organic compounds showed promising inhibiting properties for steel exposed to hydrochloric acid environment. For instance, Fouda *et al.* [29] reported that 1-[(5-mercapto-1*H*-1,2,4-triazole-3-yl)diazenyl]naphthalene-2-ol (HL) and its Mn complex exhibited good inhibition efficiencies of CS in 1 M HCl, exceeding 85% for HL and 90% for Mn complex at a concentration of 18×10^{-6}. Kannan *et al.* [30] conducted various tests to study the corrosion inhibition potential of Naphthalen-2-yl Naphthalene-2-Carboxammide (NNC) on CS in 1N HCl. Their investigation exhibited 98.5% inhibition

efficiency at 150 ppm of NNC [30]. Yusoff *et al.* [31] synthesized three coumarin-azo dyes and tested their inhibition efficacy (η) on mild steel in hostile 1 M HCl medium. Results showed a prohibition activity exceeding 80% [31]. The mitigation of carbon steel corrosion by three benzonitrile azo dyes in 1 M HCl was investigated by Fouda *et al.* [32] and revealed that the compounds presented great anticorrosion characteristics. Bedair *et al.* [33] have addressed the potential of two azo derivatives, 4-((4-hydroxy-3-((4-oxo-2-thioxothiazolidin-5-ylidene)methyl)phenyl)diazinyl)benzenesulfonic acid (TODB) and 4-((3-((4,4-dimethyl-2,6-dioxocyclohexylidene)methyl)-4-hydroxyphenyl)diazinyl)benzenesulfonic acid (DODB), to hinder mild steel corrosion in 1 M HCl. The obtained findings evinced that the azo derivatives showed highest η of 94.9% and 93.6% [33]. In this paper, (*E*)-1-((4-fluorophenyl)diazenyl)naphthalen-2-ol (E4FN) compound was evaluated as a corrosion inhibitor for carbon steel (CS) in corrosive 1 M HCl solution. On one hand, the compound E4FN presents eco-friendly and sustainable attributes which aligns with modern environmental and societal concerns. On the other hand, EF4N molecular structure was designed precisely to provide higher efficiency as an inhibitor. For this purpose, various techniques such as PDP, EIS and SEM/EDS, and UV-Visible were employed to evaluate the prohibition efficiencies (% η_s) of E4FN at a temperature of 303 K. The temperature effect was studied using PDP plots, thermodynamic descriptors were assessed accordingly. To support experimental studies, we placed additional emphasis on theoretical calculations such as Density Functional Theory (DFT) and Monte Carlo (MC) simulation. DFT calculations have been used to obtain information about the relationship between the molecular structure of an inhibitor and the effect of its inhibition. Interactions between E4FN and the Fe-surface are examined using frontier molecular orbitals (*i.e.*, HOMO and LUMO), molecular electrostatic potential (MEP), as well as global reactivity descriptors, which made it possible to correlate the structural features of the studied inhibitor with their inhibition efficiencies. We also performed an MC simulation to determine how the studied inhibitor adsorbs to the metal surface in neutral form.

2. Experimental Methods

2.1. Materials

The investigated C-steel metal bar elemental composition is as follows (wt%): C (0.370), Si (0.230), Mn (0.680), Cr (0.077), S (0.016), Ti (0.011), Ni (0.059), Co (0.059), Cu (0.16), and Fe (remainder). Before being submerged in the solutions, the metal specimens are prepared by being polished under freshwater utilizing sandpaper that has incrementally finer particle sizes ranging from 150 to 1200. Following distilled water washing, acetone degreaser, and air handler drying, these samples were processed.

2.2. Chemicals

With no further refinement, all of the compounds by Sigma-Aldrich (Spain) were utilized as received. The structure of E4FN is shown in Figure 1. In order to make molar HCl solutions,

analytical commercial grade 37% HCl was diluted with twice-distilled water. The corrosion tests were conducted in a 1 M HCl solution devoid of the inhibitor and with a range of E4FN concentrations ranging from 10^{-3} M to 10^{-6} M. The electrochemical measurements were conducted in an environment of normal air with no agitation.

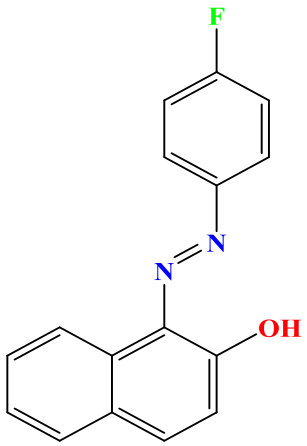

Figure 1. (*E*)-1-((4-fluorophenyl)diazenyl)naphthalen-2-ol (E4FN).

2.3. Electrochemical apparatus and measurements

A typical three-electrode cell is employed, consisting of a saturated calomel electrode (SCE) acting as a reference electrode, a platinum wire serving as the counter electrode (CE), and a steel working electrode (WE). To guarantee complete immersion of the electrodes in the cylindrical Pyrex glass cell, 90 cc of diluted hydrochloric acid were utilized. All studies were conducted at room temperature without stirring, with the exception of the impact temperature research. Using a potentiostat Volta lab PGZ 100 and Voltamaster software, electrochemical measurements (Electrochemical Impedance Spectroscopy and potentiodynamic polarization curve measurements) were made. EIS and potentiodynamic curves were used to examine the corrosion behavior of C-steel in a 1 M HCl solution in both the absence and presence of inhibitor solutions. For 30 minutes, the working electrode was immersed in the test solution to create a stable open circuit potential (E_{OCP}). The electrochemical measurements were finished after E_{OCP} measurements. Plotting of the polarization curves was done at a scanning rate of $5 \cdot 10^{-4}$ V/s in the potential range of –0.8 V to –0.1 V/SCE. By recording the electrode potential ±0.01 V versus the open circuit potential starting at a higher negative potential, measurements of linear polarization resistance were made. The voltage has been stabilized for over 30 minutes prior to all testing. The electrochemical studies are triple-realized for each inhibitor concentration, and the best results are chosen for a graphical plot. The following formula was used to compute the inhibitory efficiency (n_{PDP}(%)):

$$n_{\mathrm{PDP}}(\%) = \frac{i_{\mathrm{corr}} - i_{\mathrm{corr(inhib)}}}{i_{\mathrm{corr}}} \cdot 100 \quad (1)$$

where i_{corr} and $i_{corr(inhib)}$ symbolize, respectively, the corrosion current densities in the presence and in the absence of inhibitive chemicals. For the temperature effect component, the operating temperatures range from 303 to 333 K.

Using the same workstation previously mentioned, the electrochemical impedance spectroscopy measurements were performed at open circuit potential using an AC signal with an amplitude of 10 mV and a frequency domain of 10^5 to 10^{-2} Hz. It was done by plotting the EIS diagrams using the Nyquist and Bode representations. The ZView software 3.4 software was then used to examine the results in terms of an equivalent electrical circuit. The following formula was used to determine the inhibitory efficiency(n_{EIS}(%)):

$$n_{EIS}(\%) = \frac{R_{P(inhib)} - R_P}{R_{P(inhib)}} \cdot 100 \quad (2)$$

where $R_{P(inhib)}$ and R_P indicate, respectively, the polarization resistance values in the presence and absence of the inhibitor.

The average findings were then reported. We were able to benefit from our team's findings for both stationary and transient polarization techniques for the effect of temperature and concentration in the absence of E4FN inhibitor because we operated under the same conditions [34].

2.4. SEM explorations

SEM method has been used for surface examinations. The optimal concentration of 10^{-3} M corrosive solutions with and without inhibitive molecule was deployed. The samples were exposed to the aforementioned harsh mediums separately for 24 hours and removed delicately, rinsed with purified water, dried and then evaluated for surface morphological analysis using SEM. For the purpose of examining surface morphology, the JEOL-JSM-IT-100 model was utilized. The aforementioned metal was captured in 1000x magnification SEM pictures. We used the results of the blank in the absence and presence of HCl without inhibitor, since we worked under similar conditions in a work submitted simultaneously with this one.

2.5. UV-Vis study

The absorption UV-visible spectroscopy technique has been used to investigate the inhibitor effectiveness against corrosion. It is based on their capacity to absorb light at specific wavelengths. In order to examine how organic molecules interact with the metal surface in molar HCl solution, absorbance measurements of the solution have been carried out with and without C-steel sample being present in the acidic medium at the optimal concentration of 10^{-3} M. The wavelength scanning was done in the 200 to 600 nm range. A JASCO V-700 UV-Visible Spectrophotometer has been used.

2.6. Computational simulations details

Density Functional Theory (DFT) and Monte Carlo (MC) simulations were employed to elucidate the nature and active sites of corrosion inhibitor molecules, as well as the adsorption process on the Fe-metal surface, providing molecular-level insights.

2.6.1. DFT simulation

To establish a relationship between the predicted inhibitory efficacy of the investigated inhibitor (E4FN) and chemical reactivity indices, the DFT method was employed using the Gaussian 09 package. The calculations utilized the Becke, Lee-Yang-Parr (B3-LYP) functional [35, 36] with the 6-31G+(d, p) basis sets using the Gaussian 09 package of program [37]. Ground-state optimizations of the molecular structure of the inhibitor in an aqueous phase were performed, and various electronic properties related to the optimized parameters were investigated. These investigations included geometric parameters, as well as frontier molecular orbitals (E_{HOMO} and E_{LUMO}), and global reactivity descriptors. By analyzing the energy values of the highest occupied molecular orbital (HOMO) and lowest unoccupied molecular orbital (LUMO), several important global chemical descriptors were calculated. These descriptors include the gap energy ($\Delta E = E_{LUMO} - E_{HOMO}$), the electron affinity (A), the ionization potential (I), the dipole moment (μ) the electronegativity (χ), the chemical potential (μ), the chemical hardness (η), the softness (S), the electrophilicity index (ω), the nucleophilicity index (ε), the fraction of transferred electrons (ΔN) and metal/inhibitor interaction energy ($\Delta\psi$) were calculated according to Equations (3–12) as reported in the literature [38–41].

$$A = -E_{LUMO} \tag{3}$$

$$I = -E_{HOMO} \tag{4}$$

$$\Delta E_{gap} = E_{LUMO} - E_{HOMO} \tag{5}$$

$$\chi = \frac{(I + A)}{2} \tag{6}$$

$$\eta = \frac{(I - A)}{2} \tag{7}$$

$$S = \frac{1}{\eta} \tag{8}$$

$$\omega = \frac{\phi}{2\psi} \tag{9}$$

$$\varepsilon = \frac{1}{\omega} \tag{10}$$

$$\Delta N = \frac{\phi_{Fe} - \chi_{inhibitor}}{2\left(\eta_{Fe} + \eta_{inhibitor}\right)} \tag{11}$$

$$\Delta\psi = \frac{\left(\phi_{Fe} - \chi_{inhibitor}\right)^2}{4\left(\eta_{Fe} + \eta_{inhibitor}\right)} \tag{12}$$

where ϕ_{Fe} is the work function (4.81 eV·mol^{-1}) of iron surface (Fe(110)) which is reported to have higher stabilization energy and η_{Fe} is the absolute hardness of iron (η_{Fe}=0 eV·mol^{-1}) [39]. The frontier molecular orbitals (FMOs) distribution and molecular electrostatic potential (MEP) map were also calculated.

2.6.2. Monte Carlo simulation approach

To achieve a better understanding of the interaction between the studied inhibitor molecule (E4FN) in its neutral form onto Fe-substrate was investigated by using a Monte Carlo simulation (MC) simulation study using Material Studio 8.0 software from the BIOVIA company. The simulation of intramolecular interactions inhibitor- Fe-surface was carried out with a Fe(110) supercell of size (14×14) and a vacuum slab with (4.0 nm) thickness in a simulation box (3.4 nm×3.4 nm×6.8 nm) with periodic boundary conditions to simulate the current effective part of the Fe-substrate, without any arbitrary boundary effects [42, 43]. In the literature, it has been reported that the selected crystalline surface Fe(110) is the most stable surface among other iron surfaces such as Fe(100) and Fe(111), *etc.* [44, 45]. Furthermore, utilizing MC simulations in gas-phase and aqueous-phase adsorption onto the Fe-substrate was investigated. To simulate the aqueous-phase, the medium was composed of 500 water (H_2O) molecules, 5 corrosive hydronium (H_3O^+) and 5 chloride (Cl^-) ions, as well as the neutral structure (E4FN) of the inhibitor. The MC simulations were performed using the Universal force field to optimize the structures for our systems [46]. The Andersen thermostat kept the temperature at 303 K. Electrostatic and van der Waals parameters were both tuned to the atom-based summation method and Ewald summation method, respectively, with a cutoff distance of 18.5 Å [47].

3. Results and Discussion

3.1. Electrochemical tests

3.1.1. PDP outcomes

PDP curves were plotted for carbon steel in 1 M HCl in absence and presence of varying E4FN concentrations. As it can be seen in Figure 2, the introduction of E4FN to the medium induces a remarkable subsidence in both anodic and cathodic current densities, which emphasizes the attenuation of CS anodic dissolution and the cathodic generation of H_2. In

presence and absence of E4FN, the cathodic branches exhibit Tafel lines, implying that the addition of the inhibitor does not alter the mechanism of H^+ reduction. The latter occurs primarily through electron transfer process [48]. As for the anodic curves, two main Tafel slopes can be noticed (β_{a1} and β_{a2}). Firstly, the anodic current densities increase as the potential becomes more anodic. Then, as the potential reaches the desorption potential E_{dsp}, one may notice a sharp rise of anodic current densities followed by a flat. This behaviour may be related to the displacement of adsorption-desorption equilibrium towards the desorption of E4FN molecules from CS substrate [49]. Analysis of Table 1 shows a progressive subsidence of i_{corr} values as E4FN concentration rises in the studied medium, coupled with a displacement of E_{corr} towards more cathodic values. Riggs claimed that organic products may be classified as anodic or cathodic inhibitors in case E_{corr} shifts at least 85 mV regarding the potential found in the blank test solution [50]. In this work, the differences of E_{corr} values (ΔE_{corr}=20.2 mV for the system {CS/1 M HCl/10^{-3}M E4FN} are lower than 85 mV, emphasizing the mixed nature of E4FN [51–53]. The inhibition activities η_{PDP}(%), estimated from PDP plots according to Equation (1), increase considerably with the increment of E4FN concentration, reaching maximal a value of η_{PDP}(%)=94.4% for an optimal concentration of 10^{-3} M. The abovementioned findings further substantiate that the adsorption of E4FN on Fe-CS/1MHCl system may proficiently block the active centers on CS and subsequently impedes corrosion.

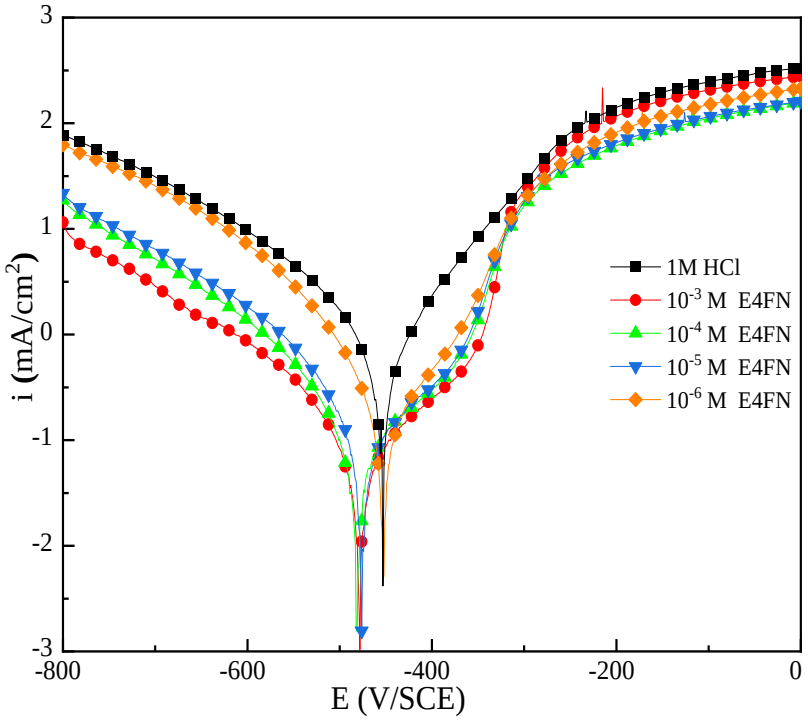

Figure 2. PDP plots for carbon steel in 1 M HCl in absence and presence of diverse concentrations of E4FN.

Table 1. Potentiodynamic polarization descriptors for carbon steel in 1 M HCl without and with various 4F concentrations at 303 K.

Medium	Concentration	$-E_{corr}$ (mV *vs.* SCE)	i_{corr} ($\mu A \cdot cm^{-2}$)	η_{PDP} (%)
Blank	1 M	456.3	1104	–
E4FN	10^{-3}	476.5	61.5	94.4
	10^{-4}	479.0	71.9	93.5
	10^{-5}	472.6	85.5	92.3
	10^{-6}	452.5	200.1	81.8

3.1.2. EIS data

EIS measurements were employed to evaluate the efficiency of E4FN inhibitor, give further insights into the different corrosion processes and examine the reaction mechanisms in the electrochemical interface. Figure 3 depicts the Nyquist representation of EIS data for CS in 1 M HCl at 303 K in presence and absence of E4FN. The addition of E4FN to the test solution leads to a considerable increment of the capacitive loops if compared to the reference solution. The radius of each spectrum depends strongly on E4FN concentration in the medium. However, the overall feature of the loops (with or without E4FN) does not undergo any changes. Such diagrams are representative of a corrosion reaction controlled by a single electron transfer [54]. All Nyquist spectra exhibit a unique depressed capacitive loop which can be related to various inputs such as surface coarseness, crystal lattice defects and porosity, impurities and the distribution of active canters [55, 56]. Figure 4 illustrates the Bode representation of EIS spectra collected for CS in 1 M HCl with and without varying concentrations of E4FN. Bode-phase plots evince as well the presence of a single capacitive time constant. At high frequency region, $\log|Z|$ and phase angle (θ) values fall to nearly zero, which is consistent with resistive conduct and may be ascribed to the resistance of the electrolyte. For midrange frequency regions, a linear correlation exists between $\log|Z|$ and $\log f$, yielding a slope below -1 and a θ inferior $-90°$. Optimally, a pure capacitor is characterized by a slope of -1 and θ of $-90°$. The noted deviation in our case is ascribed to the deceleration of the dissolution rate over time [57]. Lastly, within the low frequency range, the resistive conduct of the electrode improves and $\log|Z|$ starts to become independent of the frequency [58]. The electrical equivalent circuit (EEC) depicted in Figure 3b encloses a solution resistance R_s, a polarization resistance R_p, and a Constant Phase Element (CPE) that represents the double-layer capacitance (C_{dl}). In the electrical circuit, the CPE was involved instead of a pure capacitor to properly match the EIS data and better analyze the electrochemical processes occurring on the interface [59]. The impedance function of a CPE is described by Equation (13):

$$Z_{CPE} = Q^{-1}(i\omega)^{-n} \quad (13)$$

where Q, i, ω, and n denote respectively the CPE constant, imaginary number ($i^2=-1$), angular frequency ($\omega=2\pi f$), and phase shift. n designates the divergence with respect to the ideal conduct, comprised between 0 and 1. As claimed by Macdonald *et al.* [60], the value of n gives an indication on the substrate heterogeneity. For instance, n is homologous to a resistance when $n=0$, a capacitor for $n=1$, and assigned to a diffusion process in case $n=0.5$.

From CPE parameters, C_{dl} values were assessed according to Equation (14):

$$C_{dl} = \left(Q \cdot R_p^{1-n}\right)^{\frac{1}{n}} \tag{14}$$

Table 2 gathers the EIS descriptors previously cited (R_p, n, C_{dl}). The fitting of the impedance data points out that the value of the polarization resistance is enhanced with E4FN concentration. For instance, the presence of 10^{-3} M of E4FN raises R_p 20 times if compared to the blank solution. This can be associated with a sluggish mechanism of corrosion induced by a deficiency in active sites where the corrosion reaction could proceed. The values of n exhibit a minor increment from 0.845 to 0.85 in absence and presence of 10^{-3} M E4FN, respectively. This indicates that the surface heterogeneity slightly decreases as a result of the inhibitor adsorption. Moreover, a remarkable decline of C_{dl} values is observed as E4FN concentration gradually increases from 116.2 to 54 $\mu F \cdot cm^{-2}$ in the absence and presence of 10^{-3} M E4FN, respectively. This tendency is ascribed to a decrease of local dielectric constant and/or increment of the electrical double layer thickness. In other words, E4FN molecules are adsorbed progressively on CS surface and replace the initial components, which results in turn to a decrease of the number of active centers typically involved in corrosion in HCl solution [61].

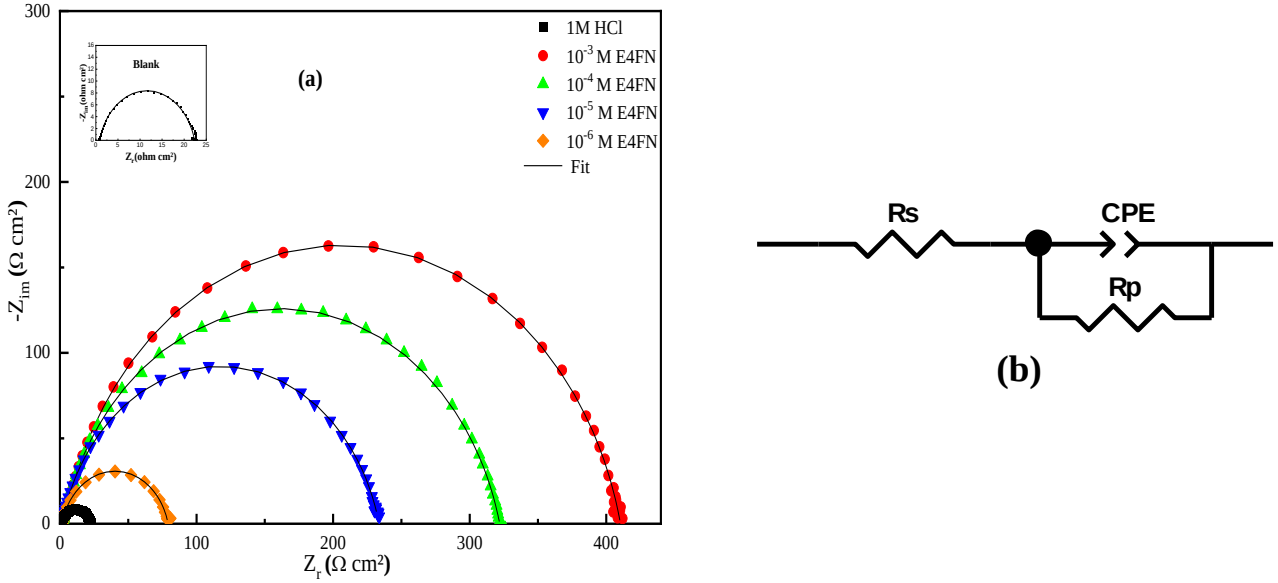

Figure 3. (a) Nyquist diagrams of carbon steel in inhibitor free 1 M HCl solution and with the addition of various concentrations of E4FN at 303 K and (b) the corresponding electrical circuit employed for fitting EIS spectra.

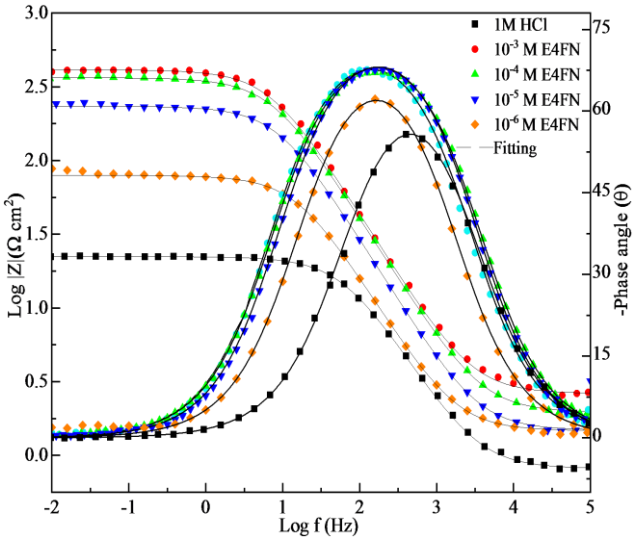

Figure 4. Bode plots and phase at 303 K for carbon steel in 1 M HCl solution in the absence and presence of various concentrations of E4FN.

Table 2. Electrochemical impedance descriptors of carbon steel in 1 M HCl solution comprising various concentrations of E4FN at 303 K.

Medium	C (M)	R_s ($\Omega \cdot cm^2$)	R_p ($\Omega \cdot cm^2$)	C_{dl} ($\mu F \cdot cm^{-2}$)	Q ($\Omega^{-1} s^n \cdot cm^{-2}$)	n_{dl}	η_{EIS} (%)
HCl	1M	0.8	21.5	116.2	293.9	0.845	–
E4FN	10^{-3}	2.7	412.2	54.0	95.6	0.850	94.8
	10^{-4}	1.9	320.1	76.4	134.4	0.848	93.3
	10^{-5}	1.5	232.3	89.4	137.6	0.854	90.7
	10^{-6}	1.5	78.7	113.6	230.7	0.850	78.1

3.1.3. Effect of temperature

In previous researches, it has been approved that temperature alters ominously the conduct of metals in aggressive environments as well as the interaction between the metallic substrate and the inhibitory products. Hence, to evaluate the impact of temperature on the potency of E4FN as an inhibitor for CS, PDP curves were drawn after ½ h of immersion time in 1 M HCl with and without 10^{-3} M of E4FN at temperatures in the range of 303–333 K (Figures 5, 6). The electrochemical descriptors assessed from PDP plots (Table 3) indicate that the increment of temperature leads to a rise of i_{corr} values in the blank test solution as well as in the presence of E4FN inhibitor, implying a decrease of η_{PDP}% values. It has been stated in earlier studies that the coarseness of metallic surfaces increases at higher temperatures [62, 63], which affects the interaction of the inhibitory molecules. Thus, it can be suggested that the observed behaviour may be the consequence of low chemical performance of E4FN molecules as the temperature raises, which induces their partial

desorption from CS surface [64]. Though, it is interesting to mention that η_{PDP}% exhibit relatively good values in the inspected temperature (η_{PDP}%=81.2% at 333 K).

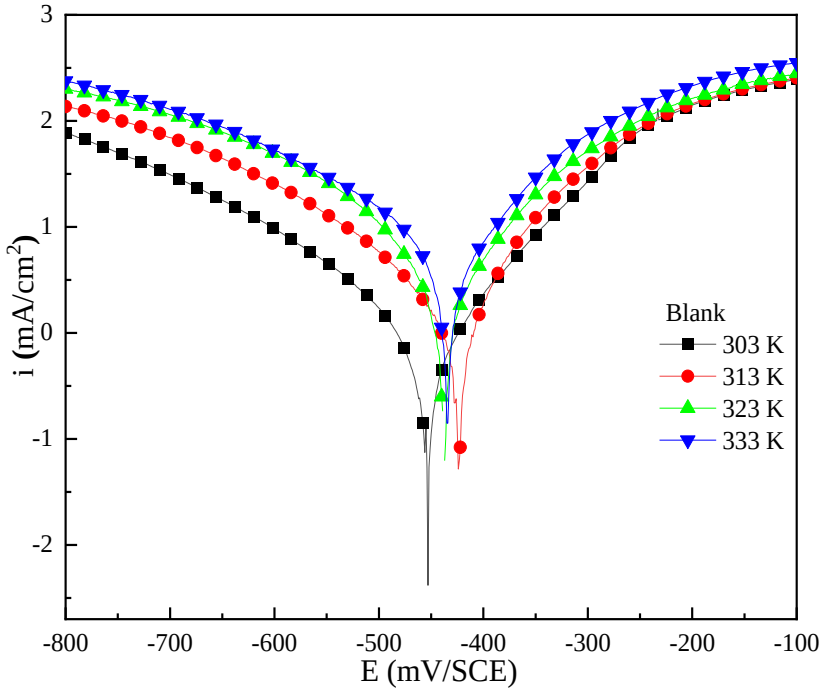

Figure 5. Potentiodynamic polarization curves for carbon steel in the absence of E4FN inhibitor at different temperatures from 303 K to 333 K.

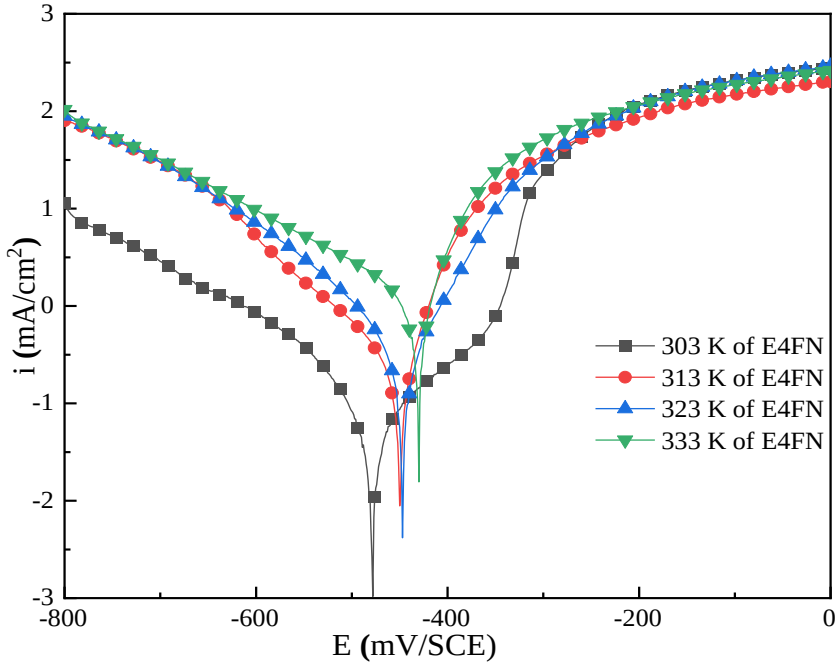

Figure 6. Potentiodynamic polarization curves for carbon steel in the present of 10^{-3} M of E4FN at different temperatures from 303 K to 333 K.

Table 3. PDP parameters for carbon steel in the present of 10^{-3} M of the blank and E4FN inhibitor at different temperatures between 303 K–333 K.

Medium	Temperature K	$-E_{corr}$ mV/SCE	i_{corr} $\mu A \cdot cm^{-2}$	η_{PDP} %
Blank	303	456.3	1104.1	–
	313	423.5	1477.4	–
	323	436.3	2254.0	–
	333	433.3	3944.9	–
E4FN	303	476.5	61.5	94.4
	313	447.0.	197.7	86.6
	323	458.3	321.4	85.7
	333	428.4	742.1	81.2

Activation thermodynamic descriptors such as E_a (activation energy), ΔH_a^* (activation enthalpy) and ΔS_a^* (activation entropy) were evaluated by examining the temperature influence as expressed by the Arrhenius law (Equation (15)) and transition state formula (Equation (16)) [52]:

$$i_{corr} = A\exp\left(\frac{-E_a}{RT}\right) \tag{15}$$

$$i_{corr} = \frac{RT}{Nh}\exp\left(\frac{\Delta S_a^*}{R}\right)\exp\left(\frac{-\Delta H_a^*}{RT}\right) \tag{16}$$

where A denotes the Arrhenius constant, R designates the gas constant, T represents the absolute temperature (K), N denotes the Avogadro's number and h stands for the Planck's constant. The respective plots are depicted in Figure 7 and Figure 8. The Arrhenius plotting exhibits straight lines whose slopes are equal to $-E_a/R$. As it can be seen in Table 4, the derived value of E_a of CS in 1 M HCl containing E4FN is higher with respect to the blank test solution. Therefore, it may be postulated that the addition of E4FN to the medium causes an increment of the energy barrier related to the corroding process. Thereby, the latter will become more challenging on CS surface and owing to the obstruction of CS active centers by E4FN molecules [65]. Moreover, positive values of ΔH_a imply that the generation of the activated complex is an endothermic process. It can also be noticed that ΔH_a is greater with the addition of E4FN to the medium, demonstrating that the corrosion of CS is mitigated by E4FN molecules. The positive increase of ΔS_a in the presence of E4FN evinces the increment of disorder of the reaction owed to the transformation from reactants to activate complexes [66].

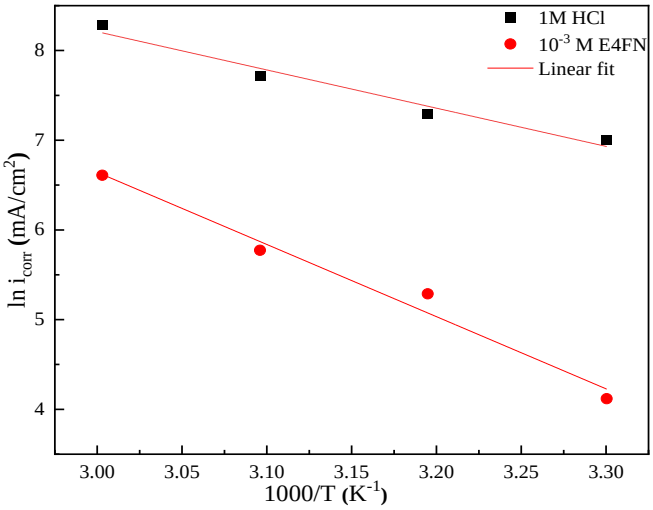

Figure 7. Arrhenius plots for carbon steel in 1 M HCl without and with 10^{-3} M of E4FN.

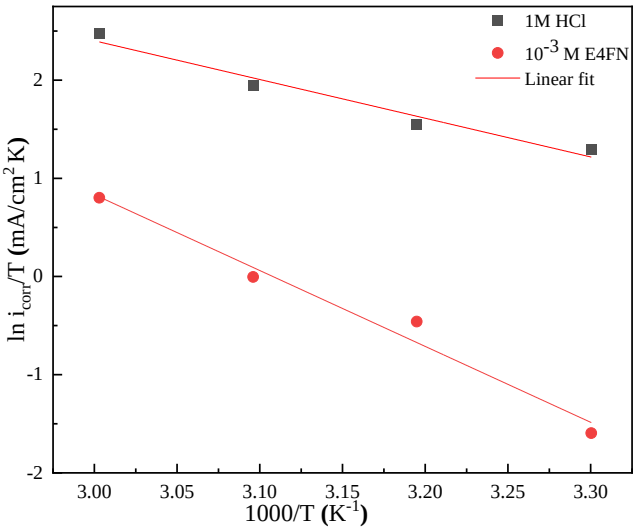

Figure 8. Transition Arrhenius plots of carbon steel in 1 M HCl with and without 10^{-3} M of E4FN.

Table 4. Activation parameters generated in 1 M HCl without and with 10^{-3} M E4FN.

Medium	E_a (kJ/mol)	ΔH_a (kJ/mol)	ΔS_a (J/mol·K)
Blank	35.41	32.77	–79.2
E4FN	66.86	64.23	2.16

3.2. Adsorption isotherm

In general, organic products interact with metallic surfaces through adsorption. Such process may be regarded as a quasi-replacement process of water molecules by the organic molecules in aqueous phase ($Org_{(aq)}$) as stated by the subsequent reaction:

$$\mathrm{Org}_{(s)} + x\mathrm{H_2O}_{(ads)} \rightarrow \mathrm{Org}_{(ads)} + x\mathrm{H_2O}_{(s)} \quad (17)$$

where x stands for the number of H_2O molecules expelled by the adsorbed inhibitors on the metallic surface. In order to unravel the adsorption mode of inhibitors, diverse adsorption isotherms (Langmuir, Temkin and Frumkin) are plotted in a way to ascertain the most appropriate one. Figure 9 depicts that the Langmuir isotherm presents an almost unitary correlation. Note that the formula expressing the Langmuir isotherm is designated by Equation (18) [67]:

$$\frac{C}{\theta} = \frac{1}{K_{ads}} + C \quad (18)$$

where K_{ads} denotes the adsorption/desorption equilibrium constant and C stands for E4FN concentration in the medium. Review of Table 5 shows a high value of K_{ads} emphasizing the potent adsorption of the inhibitor E4FN. Accordingly, it can be suggested that the investigated inhibitor is monolayer adsorbed on CS. The values of the standard adsorption free energy (ΔG_{ads}) were assessed by using Equation (19) [66]:

$$\Delta G_{ads} = -RT\ln(55.5K) \quad (19)$$

where R designates the gas constant and T stands for the absolute temperature (K). The 55.5 value designates H_2O concentration in the solution (mol/L). The negative value of ΔG_{ads} points out to the stability of the E4FN layers adsorbed on CS surface [66]. The assessed value of ΔG_{ads} is close to −40 kJ/mol (ΔG_{ads}=−45.5 kJ/mol), which indicates that a covalent bond is created (chemical adsorption) through charge transfer between E4FN and CS surface [68].

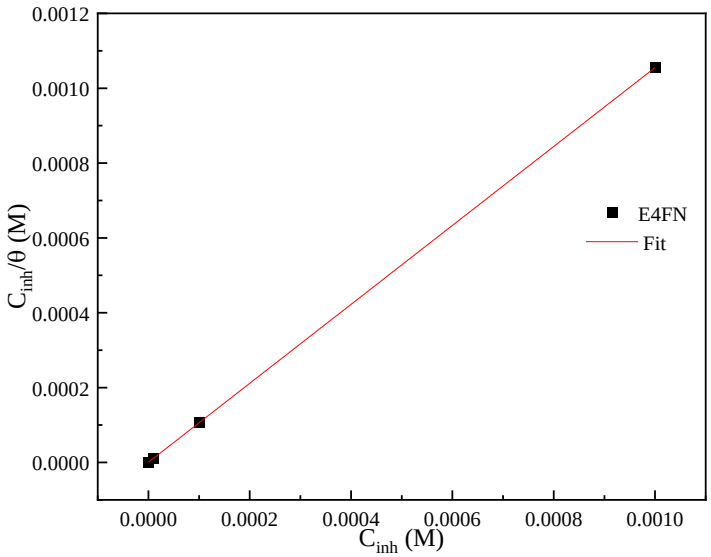

Figure 9. Langmuir adsorption isotherm plots for carbon steel in 1 M HCl in the presence of E4FN.

Table 5. Thermodynamic parameters for corrosion of carbon steel in 1 M HCl in the presence of E4FN.

Medium	K_{ads} (L/mol)	ΔG_{ads} (kJ/mol)	Slope	R^2
E4FN	1262824.0	–45.5	1.1	1.0

3.3. SEM/EDS

SEM micrographs of CS specimens were collected before (Figure 10a) and after 24 h immersion in 1 M HCl without (Figure 10b) and with the introduction of 10^{-3} M of E4FN (Figure 10c).

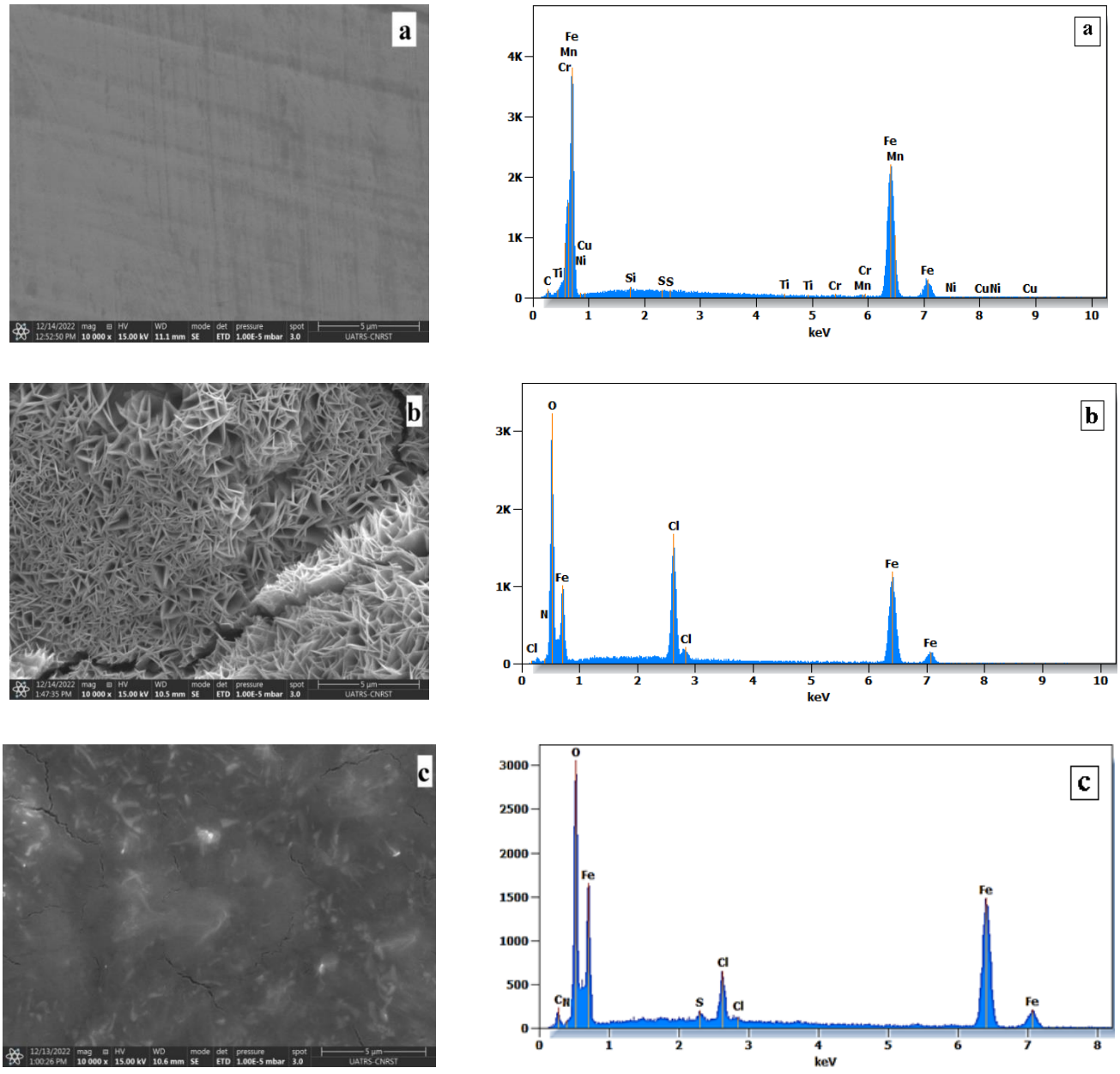

Figure 10. SEM/EDS analysis of carbon steel specimens (a) before immersion, (b) after 24 h immersion in 1 M HCl and (c) 1 M HCl+10^{-3} M of E4FN at 303 K.

As for the sanded CS, no discernible defects are apparent except for some polishing scratches. The specimen immersed in the corrosive solution is subjected to vigorous corrosion as evidenced by the development of a finely patterned rust layer (flowery structure). In 1 M HCl, the presence of intense high peaks of Cl and O atoms in EDS spectrum may be related to the formation of iron corrosion products such as $FeCl_2$ and Fe_3O_4 [69], which emphasizes the fact that CS specimen undergoes general corrosion. However, in the presence of E4FN in the solution, the morphology of CS surface is noticeably improved. As a matter of a fact, the surface becomes smooth implying the formation of a protecting layer by adsorption. The related EDS analysis evinces the occurrence of O and N atoms (adsorption of E4FN), whereas Cl peak intensity (primarily from the medium) decreases. Upon these observations, it is possible to assume that E4FN possesses significant protection abilities owed to the formation of a stable and adherent layer, which main role is to hinder electrolyte accessibility to CS surface.

3.4. UV-Visible

The interaction of CS surface and E4FN molecules was evaluated by UV-Visible spectroscopic measurements in 1 M HCl solution enclosing 10^{-3} M of E4FN before and after immersion of CS for 72 h at 303 K (Figure 11). Before the immersion of CS (black curve), the absorption curves exhibit one distinctive band around 329.2 nm. After CS immersion (red curve), the wavelength value shifts from 392.2 to 340 nm and an additional band emerges at 247.4 nm. Thus, one may assume that a complex is formed between Fe^{2+} ions and E4FN molecules in molar hydrochloric acid [70, 71].

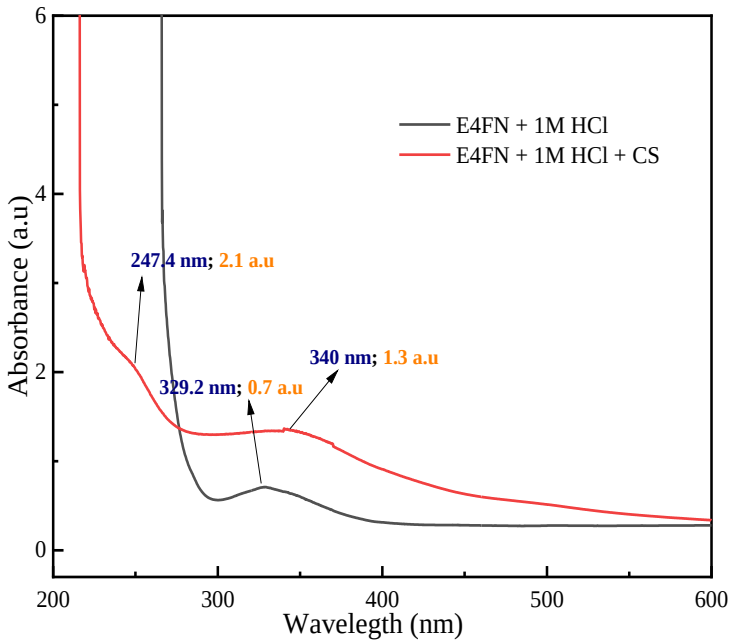

Figure 11. UV-Vis spectra of E4FN inhibitor solution before and after 3 days of immersion in 1 M HCl.

3.5. Molecular simulations

3.5.1. Protonation forms

In an acid solution, when an organic molecule containing heteroatoms is present, protonation is highly probable. Figure 12 illustrates four different protonation forms and the electronic distribution within the E4FN structure, with a form indicating that the two nitrogen atoms are the most likely sites for proton (H^+) attachment. This protonation can potentially affect the molecule's chemical reactivity while also leading to the formation of electrostatic bonds with chloride ions adsorbed on the steel surface.

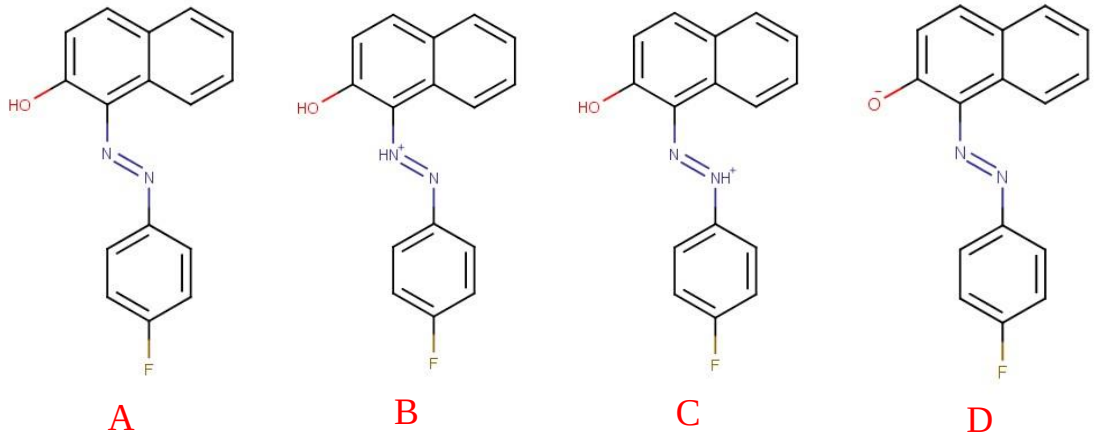

(a)

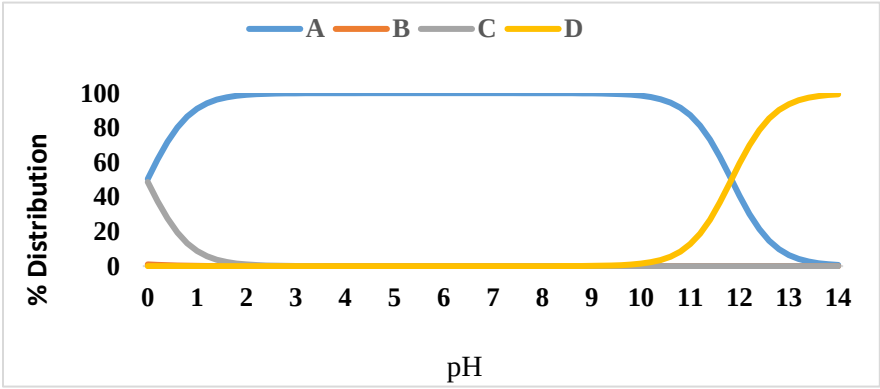

(b)

Figure 12. The different protonation forms of the E4FN (b). The electronic distribution within the E4FN structure.

3.5.2. Density functional theory (DFT) approaches

3.5.2.1. Optimized structure

DFT have indeed proven to be highly beneficial for determining molecular structures, electronic properties, and reactivity of molecules. With the remarkable advancements in supercomputing, this method has become even more powerful. Experimental techniques

used to study corrosion inhibition and understand the mechanisms can be expensive and time-consuming. Therefore, theoretical calculations employing DFT have been employed to elucidate the interactions between inhibitor molecules and Fe-surface, providing valuable insights into inhibition mechanisms. The Figure 13 illustrates the optimized molecular structure of E4FN, with labels and atoms numbering. Furthermore, the optimized molecular geometric parameters such as bond lengths and angles are shown in Table 6, were calculated using B3LYP/6-31+G(d,p) levels of theory along with the experimental data.

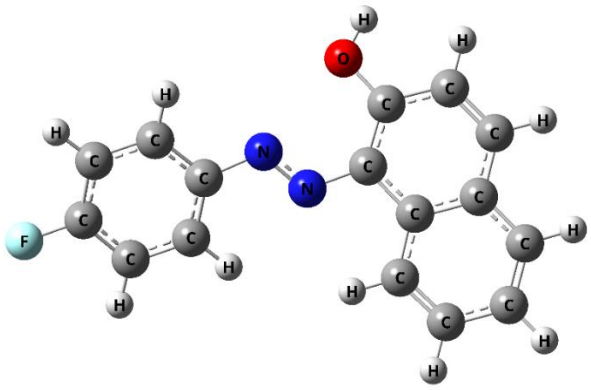

Figure 13. Optimized structure of the (E4FN) at the B3LYP/6-31+G(d,p) level of DFT calculations in aqueous phase.

3.5.2.2. Frontier molecular orbitals

Figures 14 and 15 illustrate the frontier molecular orbitals (FMO), namely HOMO and LUMO, as well as the molecular electrostatic potential (MEP) of E4FN. These figures represent the three-dimensional molecular structures in their most stable geometries, with no negative frequencies observed. The electron density distribution on the optimized structures is revealed through the HOMO and LUMO. Figure 14 demonstrates that the electron densities of LUMO and HOMO are spread across the entire molecule in its neutral state. This indicates that the structure contains electron acceptors for atoms and heteroatoms, and that the E4FN structure can be adsorbed through coordination bonds on the metallic support being studied, as well as through electrostatic bonds.

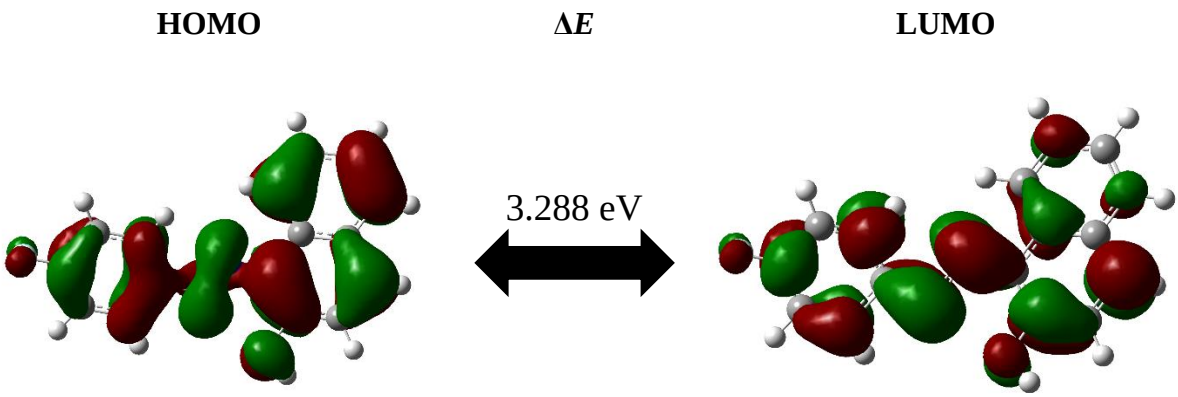

Figure 14. The contour plots of FMO for the investigated inhibitor (E4FN).

The MEP investigations provide insights into the electrophilic and nucleophilic sites of the investigated inhibitor, enabling the prediction of reactive regions. Figure 15 illustrates the MEP surfaces, where red, blue, and green colors represent the negative, positive, and neutral zones, respectively. The negative red regions are predominantly observed around the nitrogen, oxygen, and fluorine atoms. These regions indicate a higher electron density and suggest the presence of potential nucleophilic sites in the molecule.

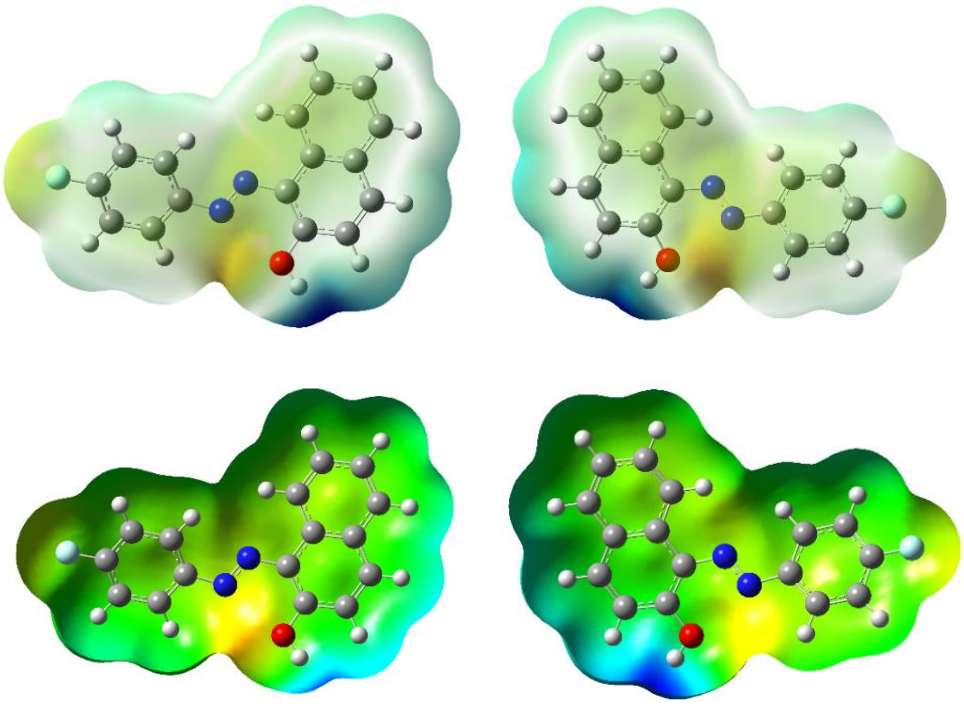

Figure 15. Molecular Electrostatic Potential (MEP) maps for the E4FN.

3.5.2.3. Global reactivity descriptors

The E_{HOMO} and E_{LUMO} values provide insights into the donor-acceptor interaction between the inhibitor molecule and the metal surface. The corrosion inhibition efficacy of the inhibitor molecule tends to increase as the E_{HOMO} becomes less negative and the E_{LUMO} becomes more negative. This indicates that the molecule becomes more capable of donating and accepting electrons from the metal surface, which is crucial for its effectiveness as a corrosion inhibitor. From the data presented in Table 6, it is evident that the form *A* of the E4FN molecule possesses a high E_{HOMO} value (−5.929 eV in aqueous phase and −5.792 eV in gas phase) and a low E_{LUMO} value (−2.641 eV in aqueous phase and −2.453 eV in gas phase), suggesting its ability to readily donate and accept electrons simultaneously.

The energy gap (ΔE), which represents the energy difference between the E_{HOMO} and E_{LUMO}, plays a crucial role in calculating various molecular properties, including optical and electronic properties, molecular stability, and, especially, in the reactivity of the inhibitor molecule during the adsorption process on the metal surface. Chemical reactivity is crucial for assessing the efficacy and structure of new inhibitors. The optimization and analysis of

the HOMO–LUMO energy gap, along with other descriptors, provide valuable information. A larger energy gap Δ*E* indicates greater kinetic stability, lower polarizability, and reduced reactivity for the E4FN (3.288 eV in aqueous phase and 3.339 in gas phase) molecule. As a result, the corrosion inhibition performance increases as the Δ*E* decreases. Therefore, a smaller energy gap corresponds to an enhanced effectiveness in inhibiting corrosion. An inhibitor with a larger hardness (η) value exhibits a greater propensity to interact with the metal surface. The η value relates to the polarizability of the inhibitor molecule, with a larger η value indicating higher polarizability and a higher likelihood of interaction with the metal surface. Conversely, inhibitors with lower η values would have a lower tendency to interact with the metal surface. Based on the findings presented in our previous works [14, 25, 51, 52, 66–68], it can be concluded that the hardness of the investigated inhibitor molecule falls within acceptable ranges (η=1.644 eV in aqueous phase and 1.700 eV in gas phase). This indicates that the E4FN molecule possesses favorable anticorrosive properties and has the potential to effectively inhibit corrosion of Fe-metal. These results suggest that the E4FN molecule holds promise as a corrosion inhibitor. The electronegativity (χ) of a molecule serves as a descriptor that indicates its ability to attract electrons. A higher χ value signifies a stronger electron-attracting effect. Conversely, a lower χ value reflects a greater propensity to donate electrons more easily. In the case of the E4FN molecule with a lower χ value (χ=4.285 eV in aqueous phase and 4.123 eV in gas phase), it suggests that E4FN interacts more favorably with the metal surface, especially when the metal surface, such as iron (χ_{Fe}=4.820 eV), has a higher electronegativity value. This implies that the E4FN molecule can readily donate electrons to the metal surface, contributing to its potential as an effective corrosion inhibitor.

Table 6. Optimization energies, HOMO and LUMO energies and their gap calculated in gas phase at B3LYP/6-31+G(d,p) level of DFT calculations.

Descriptor	**DFT**	
	Gas phase	**Aqueous phase**
E_{HOMO} (eV)	–5.792	–5.929
E_{LUMO} (eV)	–2.453	–2.641
ΔE_{gap} (eV)	3.339	3.288
I (eV)	5.792	5.929
A (eV)	2.453	2.641
χ (eV)	4.122	4.285
η (eV)	1.669	1.644
S (eV^{-1})	0.598	0.608
ω (eV)	5.089	5.584

Descriptor	DFT	
	Gas phase	Aqueous phase
ε (eV^{-1})	0.196	0.179
Δ*N*	0.205	0.159
Δψ	0.070	0.041

3.5.3. MC Simulations

In recent years, Monte Carlo (MC) Simulation has become a contemporary tool for exploring metal/inhibitor interactions [72, 73]. The interaction properties of the studied inhibitor in the neutral form (*i.e*., E4FN) on the Fe-surface in both the gas-aqueous phases are important main objectives during this part of our studies. Figure 16 shows the leading cells of E4FN on the iron (110) substrate in the gas-aqueous phases, as well as the temperature is fixed in 303 K. As can be seen in Figure 16, the E4FN is oriented parallel to Fe-atoms in gas/aqueous phases following adsorption by a large part of the carbon (C) atoms, as well as the oxygen (O) and Nitrogen (N) atoms. These atoms serve as reactive sites when the adsorption of the title compound with the iron (110) surface. Moreover, the E4FN structure seem to take the place of water molecules (H_2O) and corrosive species (H_3O^+/Cl^-) in an aqueous medium and provide a more stable location on the Fe-surface. Due to this propensity, water molecules have a synergistic impact when interacting with metallic surfaces [74, 75]. In addition, the E4FN structure in the HCl medium could result in additional stability of the studied inhibitor as it approaches the iron (110) substrate. The current research on adsorption systems (*i.e*., E4FN/Fe (110) and E4FN/$500H_2O/5H_3O^+/5Cl^-$/Fe(110) complexes) delivers effective adsorptions and hence a considerable inhibitory influence, confirming our experimental findings.

The different types of energetic descriptors of adsorbed E4FN in gas/aqueous phase are calculated and listed in Table 7. It is significant to mention that the higher and negative values of adsorption energy in gas phases (E_{ads}) and in aqueous phase ($E^{"}_{ads}$) indicates the stable/easier adsorption onto the Fe(110) surface, as well as higher inhibition efficiency [76, 77]. Moreover, the adsorption energy represents the energy absorbed when the expanded adsorbate (inhibitor) is adsorbed on the Fe-substrate [78]. From the Table 7, it is clear that the title molecule (E4FN) in gas/solution phases interacts strongly with the iron-based layer and then forming a protective adsorbed film. Furthermore, Table 7 demonstrates that during the gas phase (E4FN/Fe(110) Eads value equal to −171.63 kcal/mol)).While in the aqueous phase, the decline in adsorption energy is greater: $E^{"}_{ads}$ falls from −4878.20 kcal/mol for E4FN/$500H_2O/5H_3O^+/5Cl^-$/Fe(110). Accordingly, an aqueous solution enhances the adsorption of the title compound. As indicated in the literature, this is due to the increased stability of neutral form of the title molecule in the aqueous phase [79, 80]. In sum, the results of the MC reveal the anti-corrosion action capacity of the title

molecule (E4FN) in the gaseous and aqueous phases. These data agree with the experimental results.

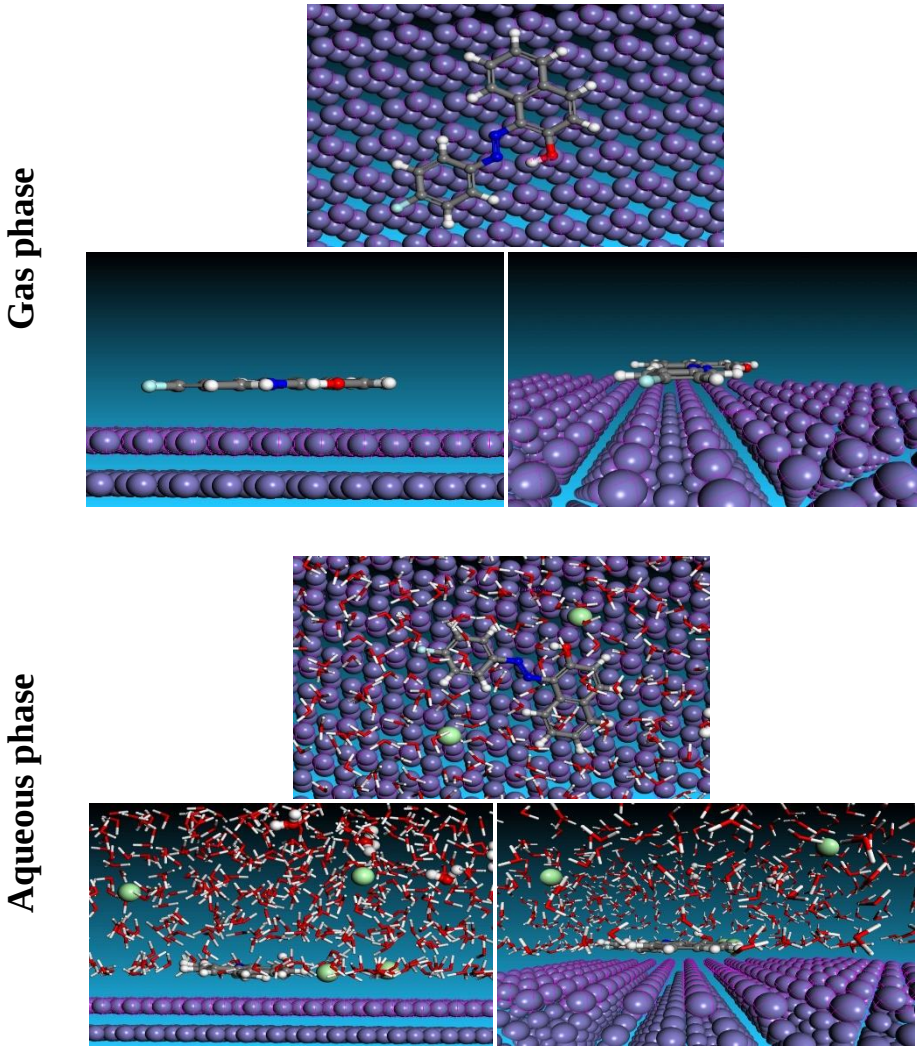

Figure 16 Upper and lateral outlooks of minimized adsorption configuration of E4FN in gas/aqueous phases over the Fe (110) surface at 303 K.

The radial distribution function (RDF) approach based on the trajectories generated by MC Simulation is employed to define the type of bonds undertaken formed at the level of the inhibitor/Fe-substrate interface. These bonds might be either physical, chemical, or both [81]. Adsorption is normally handled by chemisorption if the bond length value is between 1–3.5 Å, while the physisorption (Van der Waals and Coulomb interactions) is normally current at a bond length value >3.5 Å [82]. Figure 17 shows the RDF of E4FN in gas/solution phases. As shown in Figure 17, all of the first peak values for E4FN in the gas/solution phases are within the chemisorption range (less than 3.55 A), While other peaks outside of 3.5 A are ascribed to physical interactions. these represent the most important interactions of the simulated structures of the title molecule on the first layer of Fe atoms,

revealing that the neutral form of the title molecule does indeed hinder the disintegration of the tested steel.

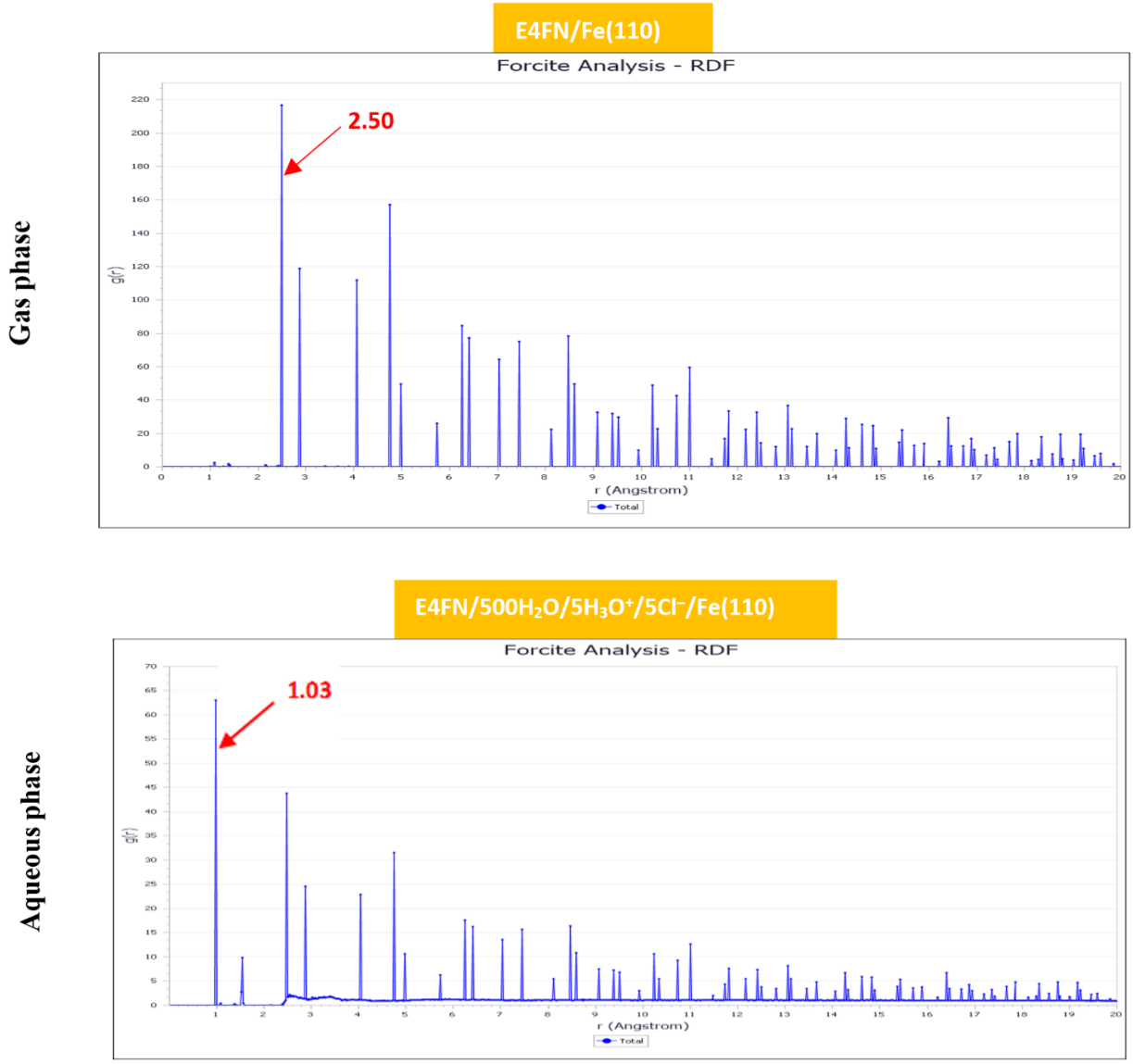

Figure 17. the RDFs of E4FN in gas/ aqueous phases over the Fe (110) surface at 303 K.

Table 7. MC simulations descriptors for the adsorption of E4FN in gas/ aqueous phases over the Fe(110) surface at 303 K (all values in Kcal/mol).

System	E_{tot}	E_{ads}	E_{RA}	E_{def}	$dE_{ads}/dN_{inhib.}$	$dE_{ads}/d\mathrm{Ni}_{H_2O}$	$dE_{ads}/d\mathrm{Ni}_{H_3O^+}$	dE_{ads}/dNi_{Cl^-}
Gas phase								
E4FN/ Fe(110)	40.17	-171.63	–5.88	–165.75	–171.63	–	–	–

System	E_{tot}	E_{ads}	E_{RA}	E_{def}	$dE_{ads}/dN_{inhib.}$	$dE_{ads}/d\mathrm{Ni}_{H_2O}$	$dE_{ads}/d\mathrm{Ni}_{H_3O^+}$	dE_{ads}/dNi_{Cl^-}
Aqueous phase								
E4FN/ 500H_2O/ 5H_3O^+/5Cl^- /Fe(110)	–3980.23	–4878.20	–4112.33	–765.86	–200.73	–11.03	–16.44	–1.23

4. Conclusion

The design and synthesis of high-performance corrosion inhibitors, which typically have larger surface coverage, more hydrophobicity, and superior adsorption capacity on the surface of metal matrix, are currently one of the most targeted areas in the field of anticorrosion. Therefore, all of these essential characteristics should be present in a great corrosion inhibitor molecule. In this work, the results obtained verified that the E4FN inhibitor has excellent corrosion inhibition performance on carbon steel in 1 M HCl medium. The corrosion inhibition efficiency is positively correlated with the PBPE concentration and negatively correlated with the experimental temperature, with the highest corrosion inhibition efficiency of 94.8%. in 1 M HCl medium containing 1 mM E4FN at 303 K. Potentiodynamic polarization disclosed clearly that E4FN is a mixed-type inhibitor and adsorbed on the surface both anodic and cathodic electrodes. EIS measurement also demonstrated that the codependent decreases of double layer capacitance with the increasing E4FN concentration which may be ascribed to the decline of the local dielectric constant at the interface of metal / solution due to the adsorption of E4FN on the metallic surface. EDS-SEM and UV-Visible analyses also confirmed that the E4FN inhibitor forms a dense and stable film on the metallic surface. These results are in good agreement with DFT calculations which showed a good relationship between the molecular structure of E4FN and its inhibition efficiency. Through to all the experimental and computational investigations, we have discovered a new and effective corrosion inhibitor on carbon steel in 1 M HCl solution: E4FN.

References

1. L. Zhang, X. Liu, X. Su, C. Lai, L. Peng, H. Zhu, L. Zhou and W. Zhang, A Dialkyldithiophosphate Derivative as Mild Steel Corrosion Inhibitor in Sulfuric Acid Solution, *Int. J. Electrochem. Sci.*, 2016, **11**, no. 7, 4828–4839. doi: 10.20964/2016.07.101
2. A. Gangan, M. El Sabbagh, M. Bedair, M. El-Sabbah and A. Fahmy, Plasma Power Impact on Electrochemical Performance of Low Carbon Steel Coated By Plasma Thin Teos Films, *Al-Azhar Bull. Sci.*, 2020, **31**, no. 1, 51–58. doi: 10.21608/absb.2020.111474

3. A. Dehghani, G. Bahlakeh and B. Ramezanzadeh, A detailed electrochemical/ theoretical exploration of the aqueous *Chinese gooseberry* fruit shell extract as a green and cheap corrosion inhibitor for mild steel in acidic solution, *J. Mol. Liq*., 2019, **282**, 366–384. doi: 10.1016/j.molliq.2019.03.011
4. Ya.G. Avdeev, T.E. Andreeva and K.L. Anfilov, Effect of some organic surfactants on the corrosion behavior of low-carbon steel in hydrochloric acid solution, *Int. J. Corros. Scale Inhib*., 2023, **12**, no. 3, 1052–1064. doi: 10.17675/2305-6894-2023-12-3-15
5. B. Liao, Z. Luo, S. Wan and L. Chen, Insight into the anti-corrosion performance of Acanthopanax senticosus leaf extract as eco-friendly corrosion inhibitor for carbon steel in acidic medium, *J. Ind. Eng. Chem*., 2023, **117**, 238–246. doi: 10.1016/j.jiec.2022.10.010
6. A. Singh, K.R. Ansari, I.H. Ali, Y. Lin, M. Murmu and P. Banerjee, Evaluation of corrosion mitigation properties of pyridinium-based ionic liquids on carbon steel in 15% HCl under the hydrodynamic condition: Experimental, surface, and computational approaches, *J. Mol. Liq*., 2023, **376**, 121408. doi: 10.1016/j.molliq.2023.121408
7. A. Zarrouk, H. Zarrok, R. Salghi, N. Bouroumane, B. Hammouti, S.S. Al-Deyab and R. Touzani, The Adsorption and Corrosion Inhibition of 2-[Bis-(3,5- dimethyl-pyrazol-1-ylmethyl)-amino]-pentanedioic Acid on Carbon Steel Corrosion in 1.0 m HCl, *Int. J. Electrochem. Sci*., 2012, **7**, no. 10, 10215–10232. doi: 10.1016/S1452-3981(23)16271-7
8. S. Zhang, Z. Tao, W. Li and B. Hou, The effect of some triazole derivatives as inhibitors for the corrosion of mild steel in 1 M hydrochloric acid, *Appl. Surf. Sci*., 2009, **255**, no. 15, 6757–6763. doi: 10.1016/j.apsusc.2008.09.089
9. L. Guo, I.B. Obot, X. Zheng, X. Shen, Y. Qiang, S. Kaya and C. Kaya, Theoretical insight into an empirical rule about organic corrosion inhibitors containing nitrogen, oxygen, and sulfur atoms, *Appl. Surf. Sci*., 2017, **406**, 301–306. doi: 10.1016/j.apsusc.2017.02.134
10. C.G. Dariva and A.F. Galio, Corrosion inhibitors–principles, mechanisms and applications, *Dev. Corros. Prot*., 2014, **16**, 365–378. doi: 10.5772/57255
11. L. Feng, S. Zhang, Y. Feng, X. Ren, H. Lu, B. Tan and S. Chen, Self-aggregate nanoscale copolymer of new synthesized compounds efficiently protecting copper corrosion in sulfuric acid solution, *Chem. Eng. J*., 2020, **394**, 124909. doi: 10.1016/j.cej.2020.124909
12. N. Mechbal, M.E. Belghiti, N. Benzbiria, C.H. Lai, Y. Kaddouri, Y. Karzazi, R. Touzani and M. Zertoubi, Correlation between corrosion inhibition efficiency in sulfuric acid medium and the molecular structures of two newly eco-friendly pyrazole derivatives on iron oxide surface, *J. Mol. Liq*., 2021, **331**, 115656. doi: 10.1016/j.molliq.2021.115656
13. D.A. Winkler, Predicting the performance of organic corrosion inhibitors, *Metals*, 2017, **7**, no. 12, 553. doi: 10.3390/met7120553

14. N. Benzbiria, A. Thoume, S. Echihi, M.E. Belghiti, A. Elmakssoudi, A. Zarrouk, M. Azzi and M. Zertoubi, Coupling of experimental and theoretical studies to apprehend the action of benzodiazepine derivative as a corrosion inhibitor of carbon steel in 1 M HCl, *J. Mol. Struct*., 2023, **1281**, 135139. doi: 10.1016/j.molstruc.2023.135139
15. W. Zhang, R. Ma, H. Liu, Y. Liu, S. Li and L. Niu, Electrochemical and surface analysis studies of 2-(quinolin-2-yl) quinazolin-4(3*H*)-one as corrosion inhibitor for Q235 steel in hydrochloric acid, *J. Mol. Liq*., 2016, **222**, 671–679. doi: 10.1016/j.molliq.2016.07.119
16. M. Kosian, M.M.J. Smulders and H. Zuilhof, Structure and long-term stability of alkylphosphonic acid monolayers on SS316L stainless steel, *Langmuir*, 2016, **32**, no. 4, 1047–1057. doi: 10.1021/acs.langmuir.5b04217
17. P. Balan, M.J. Shelton, D.O.L. Ching, G.C. Han and L.K. Palniandy, Modified silane films for corrosion protection of mild steel, *Procedia Mater. Sci*., 2014, **6**, 244–248. doi: 10.1016/j.mspro.2014.07.030
18. A. Fahmy, M. El Sabbagh, M. Bedair, A. Gangan, M. El-Sabbah, S.M. El-Bahy and J.F. Friedrich, One-step plasma deposited thin SiO_xC_y films for corrosion resistance of low carbon steel, *J. Adhes. Sci. Technol*., 2021, **35**, 1734–1751. doi: 10.1080/01694243.2020.1856539
19. F.I. Podvorica, C. Combellas, M. Delamar, F. Kanoufi and J. Pinson, Spontaneous grafting of iron surfaces by reduction of aryldiazonium salts in acidic water. Applications to the inhibition of iron corrosion, *Chem. Mater*., 2005, **17**, 3968–3975. doi: 10.1021/cm050339q
20. A. Adenier, M.C. Bernard, M.M. Chehimi, E. Cabet-Deliry, B. Desbat, O. Fagebaume, J. Pinson and F. Podvorica, Covalent modification of iron surfaces by electrochemical reduction of aryldiazonium salts, *J. Am. Chem. Soc*., 2001, **123**, no. 19, 4541–4549. doi: 10.1021/ja003276f
21. S.S. Alarfaji, I.H. Ali, M.Z. Bani-Fwaz and M.A. Bedair, Synthesis and assessment of two malonyl dihydrazide derivatives as corrosion inhibitors for carbon steel in acidic media: Experimental and theoretical studies, *Molecules*, 2021, **26**, no. 11, 3183. doi: 10.3390/molecules26113183
22. M.M. Abdelsalam, M.A. Bedair, A.M. Hassan, B.H. Heakal, A. Younis, Z.I. Elbialy, M.A. Badawy, H.E.D. Fawzy and S.A. Fareed, Green synthesis, electrochemical, and DFT studies on the corrosion inhibition of steel by some novel triazole Schiff base derivatives in hydrochloric acid solution, *Arabian J. Chem*., 2022, **15**, 103491. doi: 10.1016/j.arabjc.2021.103491
23. M.A. Abbas, M.A. Bedair, O.E. El-Azabawy and E.S. Gad, Anticorrosion Effect of Ethoxylate Sulfanilamide Compounds on Carbon Steel in 1 M Hydrochloric Acid: Electrochemical and Theoretical Studies, *ACS Omega*, 2021, **6**, no. 23, 15089–15102. doi: 10.1021/acsomega.1c01274

24. A. Zarrouk, T. Chelfi, A. Dafali, B. Hammouti, S.S. Al-Deyab, I. Warad, N. Benchat and M. Zertoubi, Comparative Study of new Pyridazine Derivatives Towards Corrosion of Copper in Nitric Acid: Part-1, *Int. J. Electrochem. Sci*., 2010, **5**, 696–705. doi: 10.1016/S1452-3981(23)15316-8
25. N. Benzbiria, S. Echihi, M.E. Belghiti, A. Thoume, A. Elmakssoudi, A. Zarrouk, M. Zertoubi and M. Azzi, Novel synthetized benzodiazepine as efficient corrosion inhibitor for copper in 3.5% NaCl solution, *Mater. Today: Proc*., 2021, **37**, 3932–3939. doi: 10.1016/j.matpr.2020.09.030
26. H. Zarrok, A. Zarrouk, R. Salghi, H. Oudda, B. Hammouti, M. Ebn Touhami, M. Bouachrinee and O.H. Pucci, A Combined Experimental and Theoretical Study on the Corrosion Inhibition and Adsorption Behaviour of Quinoxaline Derivative During Carbon Steel Corrosion in Hydrochloric Acid, *Port. Electrochim. Acta*, 2012, **30**, no. 6, 405–417. doi: 10.4152/pea.201206405
27. A. Zarrouk, B. Hammouti, A. Dafali and H. Zarrok, L-Cysteine methyl ester hydrochloride: A new corrosion inhibitor for copper in nitric acid, *Der Pharma Chem*., 2011, **3**, no. 4, 266–274.
28. R. Nabah, F. Benhiba, Y. Ramli, M. Ouakki, M. Cherkaoui, H. Oudda, R. Touir, I. Warad and A. Zarrouk, Corrosion Inhibition Study of 5, 5-diphenylimidazolidine2, 4-dione for Mild Steel Corrosion in 1 M HCl Solution: Experimental, Theoretical Computational and Monte Carlo Simulations Studies, *Anal. Bioanal. Electrochem*., 2018, **10**, no. 10, 1375–1398.
29. A.S. Fouda, M.A. El-Morsi, M. Gaber and M. Fakeeh, A comparative study of the corrosion inhibition of carbon steel in HCl solution by 1-[(5-mercapto-1*H*-1, 2, 4-triazole-3-yl) diazenyl] naphthalene-2-ol (HL) and its manganese complex, *Chem. Data Collect*., 2020, **28**, 100479. doi: 10.1016/j.cdc.2020.100479
30. P. Kannan, T.S. Rao and N. Rajendran, Improvement in the corrosion resistance of carbon steel in acidic condition using naphthalen-2-ylnaphthalene-2-carboxammide inhibitor, *J. Colloid Interface Sci*., 2018, **512**, 618–628. doi: 10.1016/j.jcis.2017.09.061
31. M.H. Yusoff, M.N. Azmi, M.H. Hussin, H. Osman, P.B. Raja, A.A. Rahim and K. Awang, An Electrochemical evaluation of synthesized coumarin-Azo dyes as potential corrosion inhibitors for mild steel in 1 M HCl medium, *Int. J. Electrochem. Sci*., 2020, **15**, no. 12, 11742–11756. doi: 10.20964/2020.12.43
32. A.S. Fouda, A.H. El-Azaly, R.S. Awad and A.M. Ahmed, New benzonitrile azo dyes as corrosion inhibitors for carbon steel in hydrochloric acid solutions, *Int. J. Electrochem. Sci*., 2014, **9**, 1117–1131. doi: 10.1016/S1452-3981(23)07782-9
33. M.A. Bedair, H.M. Elaryian, E.S. Gad, M. Alshareef, A.H. Bedair, R.M. Aboushahba and A.E.A.S. Fouda, Insights into the adsorption and corrosion inhibition properties of newly synthesized diazinyl derivatives for mild steel in hydrochloric acid: synthesis, electrochemical, SRB biological resistivity and quantum chemical calculations, *RSC Adv*., 2023, **13**, 478–498. doi: 10.1039/D2RA06574F

34. W. Al Garadi, K. Jrajri, M. El Faydy, F. Benhiba, L. El Ghayati, N.K. Sebbar, E.M. Essassi, I. Warad, A. Guenbour, A. Bellaouchou, C. Jama, A. Alsalme and A. Zarrouk, 4-phenyl-decahydro-1*H*-1,5-benzodiazepin-2-one as novel and effective corrosion inhibitor for carbon steel in 1 M HCl solution: a combined experimental and empirical studies, *J. Indian Chem. Soc*., 2022, **99**, no. 11, 100742. doi: 10.1016/j.jics.2022.100742
35. A.D. Becke, Becke's three parameter hybrid method using the LYP correlation functional, *J. Chem. Phys*., 1993, **98**, 5648–5652.
36. C. Lee, W. Yang and R.G. Parr, Development of the Colle-Salvetti correlation-energy formula into a functional of the electron density, *Phys. Rev*., 1988, **37**, 785–789. doi: 10.1103/PhysRevB.37.785
37. M.J. Frisch, G.W. Trucks, H.B. Schlegel, G.E. Scuseria, M.A. Robb, J.R. Cheeseman, G. Scalmani, V. Barone, B. Mennucci, G.A. Petersson, H. Nakatsuji, M. Caricato, X. Li, H.P. Hratchian, A.F. Izmaylov, J. Bloino, G. Zheng, J.L. Sonnenberg, M. Hada, M. Ehara, K. Toyota, R. Fukuda, J. Hasegawa, M. Ishida, T. Nakajima, Y. Honda, O. Kitao, H. Nakai, T. Vreven, J. Montgomery, J.E. Peralta, F. Ogliaro, M. Bearpark, J.J. Heyd, E. Brothers, K.N. Kudin, V.N. Staroverov, R. Kobayashi, J. Normand, K. Raghavachari, A. Rendell, J.C. Burant, S.S. Iyengar, J. Tomasi, M. Cossi, N. Rega, J.M. Millam, M. Klene, J.E. Knox, J.B. Cross, V. Bakken, C. Adamo, J. Jaramillo, R. Gomperts, R.E. Stratmann, O. Yazyev, A.J. Austin, R. Cammi, C. Pomelli, J.W. Ochterski, R.L. Martin, K. Morokuma, V.G. Zakrzewski, G.A. Voth, P. Salvador, J.J. Dannenberg, S. Dapprich, A.D. Daniels, Ö. Farkas, J.B. Foresman, J.V. Ortiz, J. Cioslowski and D.J. Fox, *Gaussian 09, Revision D.01*, Gaussian, Inc., Wallingford CT, 2009.
38. G. Cinar, T. Agbektas, A. Huseynzada, G. Aliyeva, M. Aghayev, U. Hasanova, S. Kaya, S. Chtita, H. Nour, A. Tas and Y. Silig, Experimental and theoretical insights about the effect of some newly designed azomethine group-contained macroheterocycles on oxidative stress and DNA repair gene profiles in neuroblastoma cell lines, *J. Mol. Struct*., 2023, **1285**, 135432. doi: 10.1016/j.molstruc.2023.135432
39. T. Agbektas, C. Zontul, A. Ozturk, A. Huseynzada, R. Ganbarova, U. Hasanova, G. Cinar, A. Tas, S. Kaya, S. Chtita and Y. Silig, Effect of azomethine group containing compounds on gene profiles in Wnt and MAPK signal patterns in lung cancer cell line: *In silico* and *in vitro* analyses, *J. Mol. Struct*., 2023, **1275**, 134619. doi: 10.1016/j.molstruc.2022.134619
40. A.S. Mohamed, I. Jourdain, M. Knorr, A. Elmi, S. Chtita, R. Scheel, C. Strohmann and M.A. Hussien, Design of hydroxyl-and thioether-functionalized iron-platinum dimetallacyclopentenone complexes. Crystal and electronic structures, Hirshfeld and docking analyses and anticancer activity evaluated by in silico simulation, *J. Mol. Struct*., 2022, **1251**, 131979. doi: 10.1016/j.molstruc.2021.131979

41. A. Zahlou, S. Chtita, M. Ghamali, L. Bejjit, T. Lakhlifi and M. Bouachrine, Electronic and photovoltaic properties of new materials based on imidazo [1, 2-a] pyrazine. Computational investigations, *Funct. Mater*., 2013, **20**, no. 4, 504–509. doi: 10.15407/fm20.04.504
42. P. Singh, E.E. Ebenso, L.O. Olasunkanmi, I.B. Obot and M.A. Quraishi, Electrochemical, theoretical, and surface morphological studies of corrosion inhibition effect of green naphthyridine derivatives on mild steel in hydrochloric acid, *J. Phys. Chem. C*., 2016, **120**, no. 6, 3408–3419. doi: 10.1021/acs.jpcc.5b11901
43. C. Verma, L.O. Olasunkanmi, E.E. Ebenso, M.A. Quraishi and I.B. Obot, Adsorption behavior of glucosamine-based, pyrimidine-fused heterocycles as green corrosion inhibitors for mild steel: experimental and theoretical studies, *J. Phys. Chem. C*., 2016, **120**, no. 21, 11598–11611. doi: 10.1021/acs.jpcc.6b04429
44. N. Asadi, M. Ramezanzadeh, G. Bahlakeh and B. Ramezanzadeh, Utilizing *Lemon Balm* extract as an effective green corrosion inhibitor for mild steel in 1 M HCl solution: A detailed experimental, molecular dynamics, Monte Carlo and quantum mechanics study, *J. Taiwan Inst. Chem. Eng*., 2019, **95**, 252–272. doi: 10.1016/j.jtice.2018.07.011
45. L.O. Olasunkanmi, I.B. Obot, M.M. Kabanda and E.E. Ebenso, Some quinoxalin-6-yl derivatives as corrosion inhibitors for mild steel in hydrochloric acid: experimental and theoretical studies, *J. Phys. Chem. C*., 2015, **119**, 16004–16019. doi: 10.1021/acs.jpcc.5b03285
46. L. Chen, D. Lu and Y. Zhang, Organic compounds as corrosion inhibitors for carbon steel in HCl solution: a comprehensive review, *Materials*, 2022, **15**, no. 6, 2023. doi: 10.3390/ma15062023
47. A. Chraka, I. Raissouni, N. Ben Seddik, S. Khayar, S. El Amrani, M. El Hadri, F. Chaouket and D. Bouchta, Croweacin and Ammi visnaga (L.) lam essential oil derivatives as green corrosion inhibitors for brass in 3% NaCl medium: quantum mechanics investigation and molecular dynamics simulation approaches, *Mediterr. J. Chem*., 2020, **10**, no. 4, 378. doi: 10.13171/mjc10402004281338ac
48. H. Derfouf, Y. Harek, L. Larabi, W.J. Basirun and M. Ladan, Corrosion inhibition activity of carbon steel in 1.0 M hydrochloric acid medium using Hammada scoparia extract: gravimetric and electrochemical study, *J. Adhes. Sci. Technol*., 2019, **33**, no. 8, 808–833. doi: 10.1080/01694243.2018.1562321
49. X. Li, X. Xie, S. Deng and G. Du, Two phenylpyrimidine derivatives as new corrosion inhibitors for cold rolled steel in hydrochloric acid solution, *Corros. Sci*., 2014, **87**, 27–39. doi: 10.1016/j.corsci.2014.05.017
50. H. Ahmed, F. Mahmoud and Z. Abdelhalim, Corrosion inhibition of X70 steel by tetrabutylammonium iodide in 1 M HCl at different temperatures, *Int. J. Corros. Scale Inhib*., 2023, **12**, no. 2, 489–510. doi: 10.17675/2305-6894-2023-12-2-7

51. Y. El Ouadi, F. Abrigach, A. Bouyanzer, R. Touzani, O. Riant, B. El Mahi, A. El Assyry, S. Radi, A. Zarrouk and B. Hammouti, Corrosion inhibition of mild steel by new N-heterocyclic compound in 1 M HCl: Experimental and computational study, *Der Pharma Chem*., 2015, **7**, no. 8, 265–275.
52. Y.E. Louadi, F. Abrigach, A. Bouyanzer, R. Touzani, A. El Assyry, A. Zarrouk and B. Hammouti, Theoretical and Experimental Studies on the Corrosion Inhibition Potentials of Two Tetrakis Pyrazole Derivatives for Mild Steel in 1.0 M HCl, *Port. Electrochim. Acta*, 2017, **35**, no. 3, 159–178. doi: 10.4152/pea.201703159
53. V.V. Torres, R.S. Amado, C.F. de Sá, T.L. Fernandez, C.A. da S. Riehl, A.G. Torres and E. D'Elia, Inhibitory action of aqueous coffee ground extracts on the corrosion of carbon steel in HCl solution, *Corros. Sci*., 2011, **53**, no. 7, 2385–2392. doi: 10.1016/j.corsci.2011.03.021
54. Y.W. Liu, Y. Chen, X.H. Chen, Z.N. Yang and Z. Zhang, Study on adsorption behavior of ketoconazole on Q235 mild steel in 1.0 M HCl solution with electrochemical measurement, *J. Alloys Compd*., 2018, **758**, 184–193. doi: 10.1016/j.jallcom.2018.05.107
55. M. Goyal, H. Vashisht, S.H. Alrefaee, R. Jain, S. Kumar, S. Kaya, L. Guo and C. Verma, Decyltriphenylphosphonium bromide containing hydrophobic alkyl-chain as a potential corrosion inhibitor for mild steel in sulfuric acid: Theoretical and experimental studies, *J. Mol. Liq*., 2021, **336**, 116166. doi: 10.1016/j.molliq.2021.116166
56. S. Cao, D. Liu, T. Wang, A. Ma, C. Liu, X. Zhuang, H. Ding, B.B. Mamba and J. Gui, Nitrogen-doped carbon dots as high-effective inhibitors for carbon steel in acidic medium, *Colloids Surf., A*, 2021, **616**, 126280. doi: 10.1016/j.colsurfa.2021.126280
57. D.K. Yadav, D.S. Chauhan, I. Ahamad and M.A. Quraishi, Electrochemical behavior of steel/acid interface: Adsorption and inhibition effect of oligomeric aniline, *RSC Adv* 2013, **3**, no. 2, 632–646. doi: 10.1039/c2ra21697c
58. M. Kissi, M. Bouklah, B. Hammouti and M. Benkaddour, Establishment of equivalent circuits from electrochemical impedance spectroscopy study of corrosion inhibition of steel by pyrazine in sulphuric acidic solution, *Appl. Surf. Sci*., 2006, **252**, no. 12, 4190–4197. doi: 10.1016/j.apsusc.2005.06.035
59. M. Zhang, L. Guo, M. Zhu, K. Wang, R. Zhang, Z. He, Y. Lin, S. Leng, V.C. Anadebe and X. Zheng, Akebia trifoliate koiaz peels extract as environmentally benign corrosion inhibitor for mild steel in HCl solutions: integrated experimental and theoretical investigations, *J. Ind. Eng. Chem*., 2021, **101**, 227–236. doi: 10.1016/j.jiec.2021.06.009
60. D.D. Macdonald, Review of mechanistic analysis by electrochemical impedance spectroscopy, *Electrochim. Acta*, 1990, **35**, 1509–1525. doi: 10.1016/0013-4686(90)80005-9

61. L.O. Olasunkanmi, N.I. Aniki, A.S. Adekunle, L.M. Durosinmi, S.S. Durodola, O.O. Wahab and E.E. Ebenso, Investigating the synergism of some hydrazinecarboxamides and iodide ions as corrosion inhibitor formulations for mild steel in hydrochloric Acid: Experimental and computational studies, *J. Mol. Liq*., 2021, **343**, 117600. doi: 10.1016/j.molliq.2021.117600
62. E. Geler and D.S. Azambuja, Corrosion inhibition of copper in chloride solutions by pyrazole, *Corros. Sci*., 2000, **42**, no. 4, 631–643. doi: 10.1016/S0010-938X(99)00080-3
63. M.E. Belghiti, M. Mihit, A. Mahsoune, A. Elmelouky, R. Mghaiouini, A. Barhoumi, A. Dafali, M. Bakasse, M.A. El Mhammedi and M. Abdennouri, Studies of Inhibition effect "E & Z" Configurations of hydrazine Derivatives on Mild Steel Surface in phosphoiric acid, *J. Mater. Res. Technol*., 2019, **8**, no. 6, 6336–6353. doi: 10.1016/j.jmrt.2019.09.051
64. A. Thoume, D.B. Left, A. Elmakssoudi, F. Benhiba, A. Zarrouk, N. Benzbiria, I. Warad, M. Dakir, M. Azzi and M. Zertoubi, Chalcone oxime derivatives as new inhibitors corrosion of carbon steel in 1 M HCl solution, *J. Mol. Liq*., 2021, **337**, 116398. doi: 10.1016/j.molliq.2021.116398
65. H.C. Andersen, Molecular dynamics simulations at constant pressure and/or temperature, *J. Chem. Phys*., 1980, **72**, no. 4, 2384–2393. doi: 10.1063/1.439486
66. A. Zarrouk, B. Hammouti, H. Zarrok, S.S. Al-Deyab and M. Messali, Temperature effect, activation energies and thermodynamic adsorption studies of Lcysteine methyl ester hydrochloride as copper corrosion inhibitor in nitric acid 2 M, *Int. J. Electrochem. Sci*., 2011, **6**, no. 12, 6261–6274. doi: 10.1016/S1452-3981(23)19679-9
67. F. Benhiba, Z. Benzekri, Y. Kerroum, N. Timoudan, R. Hsissou, A. Guenbour, M. Belfaquir, S. Boukhris, A. Bellaouchou, H. Oudda and A. Zarrouk, Assessment of inhibitory behavior of ethyl 5-cyano-4-(furan-2-yl)-2-methyl-6-oxo-1,4,5,6-tetrahydropyridine-3-carboxylate as a corrosion inhibitor for carbon steel in molar HCl: Theoretical approaches and experimental investigation, *Indian J. Appl. Chem*., 2023, **100**, no. 2, 100916. doi: 10.1016/j.jics.2023.100916
68. L. Afia, R. Salghi, A. Zarrouk, H. Zarrok, E.H. Bazzi, B. Hammouti and M. Zougagh, Comparative study of corrosion inhibition on mild steel in HCl Medium by three green compounds: *Argania spinosa* Press Cake, Kernels and Hulls Extracts, *Trans. Indian Inst. Met*., 2013, **66**, 43–49. doi: 10.1007/s12666-012-0168-z
69. M.M. Solomon and S.A. Umoren, In-situ preparation, characterization and anticorrosion property of polypropylene glycol/silver nanoparticles composite for mild steel corrosion in acid solution, *J. Colloid Interface Sci*., 2016, **462**, 29–41. doi: 10.1016/j.jcis.2015.09.057
70. M. Rbaa, M. Fardioui, C. Verma, A.S. Abousalem, M. Galai, E.E. Ebenso, T. Guedira, B. Lakhrissi, I. Warad and A. Zarrouk, 8-Hydroxyquinoline based chitosan derived carbohydrate polymer as biodegradable and sustainable acid corrosion inhibitor for mild steel: Experimental and computational analyses, *Int. J. Biol. Macromol*., 2020, **155**, 645–655. doi: 10.1016/j.ijbiomac.2020.03.200

71. S. Cao, D. Liu, P. Zhang, L. Yang, P. Yang, H. Lu and J. Gui, Green Brönsted acid ionic liquids as novel corrosion inhibitors for carbon steel in acidic medium, *Sci. Rep*., 2017, **7**, 8773. doi: 10.1038/s41598-017-07925-y
72. S. Shadi, G. Bahlakeh, B. Ramezanzadeh and A.H.J. Mofidabadi, Experimental and computational exploration of synergistic effect of *Laurus Nobilis* extract: Zinc cation on mild steel corrosion inhibition in saline solution, *J. Mol. Liq*., 2023, **385**, 122424. doi: 10.1016/j.molliq.2023.122424
73. M. Belhadi, M. Oubahou, I. Hammoudan, A. Chraka, M. Chafi and S. Tighadouini, A comprehensive assessment of carbon steel corrosion inhibition by 1, 10-phenanthroline in the acidic environment: insights from experimental and computational studies, *Environ. Sci. Pollut. Res*., 2023, 1–18. doi: 10.1007/s11356-023-27582-1
74. A. Jmiai, A. Tara, S. El Issami, M. Hilali, O. Jbara and L. Bazzi, A new trend in corrosion protection of copper in acidic medium by using Jujube shell extract as an effective green and environmentally safe corrosion inhibitor: Experimental, quantum chemistry approach and Monte Carlo simulation study, *J. Mol. Liq*., 2021, **322**, 114509. doi: 10.1016/j.molliq.2020.114509
75. S. Pareek, D. Jain, S. Hussain, A. Biswas, R. Shrivastava, S.K. Parida, H.K. Kisan, H. Lgaz, I.M. Chung and D. Behera, A new insight into corrosion inhibition mechanism of copper in aerated 3.5 wt.% NaCl solution by eco-friendly Imidazopyrimidine Dye: experimental and theoretical approach, *Chem. Eng. J*., 2019, **358**, 725–742. doi: 10.1016/j.cej.2018.08.079
76. M. Rbaa, F. Benhiba, M. Galai, A.S. Abousalem, M. Ouakki, C.H. Lai, B. Lakhrissi, C. Jama, I. Warad and M.E. Touhami, Synthesis and characterization of novel Cu (II) and Zn (II) complexes of 5-{[(2-Hydroxyethyl) sulfanyl] methyl}-8-hydroxyquinoline as effective acid corrosion inhibitor by experimental and computational testings, *Chem. Phys. Lett*., 2020, **754**, 137771. doi: 10.1016/j.cplett.2020.137771
77. A. Jmiai, B. El Ibrahimi, A. Tara, S. El Issami, O. Jbara and L. Bazzi, Alginate biopolymer as green corrosion inhibitor for copper in 1 M hydrochloric acid: experimental and theoretical approaches, *J. Mol. Struct*., 2018, **1157**, 408–417. doi: 10.1016/j.molstruc.2017.12.060
78. M. Khattabi, F. Benhiba, S. Tabti, A. Djedouani, A. El Assyry, R. Touzani, I. Warad, H. Oudda and A. Zarrouk, Performance and computational studies of two soluble pyran derivatives as corrosion inhibitors for mild steel in HCl, *J. Mol. Struct*., 2019, **1196**, 231–244. doi: 10.1016/j.molstruc.2019.06.070
79. B. El Ibrahimi, A. Jmiai, K. El Mouaden, R. Oukhrib, A. Soumoue, S. El Issami and L. Bazzi, Theoretical evaluation of some α-amino acids for corrosion inhibition of copper in acidic medium: DFT calculations, Monte Carlo simulations and QSPR studies, *J. King Saud Univ., Sci*., 2020, **32**, no. 1, 163–171. doi: 10.1016/j.jksus.2018.04.004

80. M.M. Kabanda, I.B. Obot and E.E. Ebenso, Computational study of some amino acid derivatives as potential corrosion inhibitors for different metal surfaces and in different media, *Int. J. Electrochem. Sci*., 2013, **8**, 10839–10850. doi: 10.1016/S1452-3981(23)13152-X
81. G.A. Zhang, X.M. Hou, B.S. Hou and H.F. Liu, Benzimidazole derivatives as novel inhibitors for the corrosion of mild steel in acidic solution: Experimental and theoretical studies, *J. Mol. Liq*., 2019, **278**, 413–427. doi: 10.1016/j.molliq.2019.01.060
82. V. Mehmeti and F.I. Podvorica, Experimental and theoretical studies on corrosion inhibition of niobium and tantalum surfaces by carboxylated graphene oxide, Materials, 2018, **11**, no. 6, 893. doi: 10.3390/ma11060893

♦ ♦ ♦